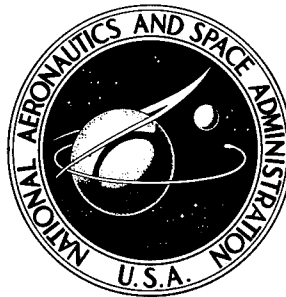


SK1  
AHL  
ADD 421854

NASA TECHNICAL NOTE



NASA TN D-8319

NASA TN D-8319

DEPARTMENT OF DEFENSE  
PLASTICS TECHNICAL EVALUATION CENTER  
PICATINNY ARSENAL, GOVTG. N. J.

# DESIGN, FABRICATION, AND STRUCTURAL TESTING OF A LIGHTWEIGHT SHADOW SHIELD FOR DEEP-SPACE APPLICATION

*David Miao, James R. Barber,  
and Richard L. DeWitt*

*Lewis Research Center  
Cleveland, Ohio 44135*

19960229 104

NATIONAL AERONAUTICS AND SPACE ADMINISTRATION • WASHINGTON, D. C. • MARCH 1977

DTIC QUALITY INSPECTED 1

PLASTEC 25021

1. Report No. <b>NASA TN D-8319</b>		2. Government Accession No.		3. Recipient's Catalog No.	
4. Title and Subtitle <b>DESIGN, FABRICATION, AND STRUCTURAL TESTING OF A LIGHTWEIGHT SHADOW SHIELD FOR DEEP-SPACE APPLICATION</b>				5. Report Date <b>March 1977</b>	
				6. Performing Organization Code	
7. Author(s) <b>David Miao, James R. Barber, and Richard L. DeWitt</b>				8. Performing Organization Report No. <b>E-8889</b>	
9. Performing Organization Name and Address <b>Lewis Research Center National Aeronautics and Space Administration Cleveland, Ohio 44135</b>				10. Work Unit No. <b>506-21</b>	
				11. Contract or Grant No.	
12. Sponsoring Agency Name and Address <b>National Aeronautics and Space Administration Washington, D. C. 20546</b>				13. Type of Report and Period Covered <b>Technical Note</b>	
				14. Sponsoring Agency Code	
15. Supplementary Notes					
16. Abstract <p>Two 3.05-meter-diameter (10-ft-diam), full-scale, lightweight, double-sheeted shadow shields were developed as the primary element of a deep-space thermal protection system for liquid-hydrogen propellant tankage. The thermal and mechanical considerations used in the design of the shields, the method of fabrication, and the environmental testing results on a prototype shield are discussed. Testing consisted of a transient cooldown period, a prolonged cold soak, and a transient warmup. The results of the tests demonstrated that the mechanical and thermal analyses used in the shield design are sufficient to produce a lightweight (i. e., 8.3 kg (18.2 lb)), rugged shadow shield assembly that is structurally adequate for its intended application.</p>					
17. Key Words (Suggested by Author(s)) <b>Cryogenic fluid storage; Space storage; Thermal insulation; Thermal protection; Solar radiation shielding; Radiation protection</b>				18. Distribution Statement <b>Unclassified - unlimited STAR Category 18</b>	
19. Security Classif. (of this report) <b>Unclassified</b>		20. Security Classif. (of this page) <b>Unclassified</b>		21. No. of Pages <b>49</b>	
				22. Price* <b>A03</b>	

# DESIGN, FABRICATION, AND STRUCTURAL TESTING OF A LIGHTWEIGHT SHADOW SHIELD FOR DEEP-SPACE APPLICATION

by David Miao, James R. Barber, and Richard L. DeWitt

Lewis Research Center

## SUMMARY

Two 3.05-meter-diameter (10-ft-diam), full-scale, lightweight, double-sheeted shadow shields were developed as the primary element of a deep-space thermal protection system for liquid-hydrogen propellant tankage. Both mechanical and thermal environmental requirements dictated the final design, which was not only practical but simple. The thermal and mechanical considerations used in the design of the shields, the method of fabrication, and the environmental testing results on a prototype shield are discussed. Testing consisted of a transient cooldown period, a prolonged cold soak, and a transient warmup.

The results of the tests demonstrated that the mechanical and thermal analyses used in the shield design are sufficient to produce a lightweight (i. e., 8.3 kg (18.2 lb)), rugged shadow shield assembly that is structurally adequate for its intended application.

The thermal performance of the shield, when used as part of a complete insulation system, has been documented elsewhere and has been shown to be satisfactory.

## INTRODUCTION

For several years, the Lewis Research Center has been engaged in experimental programs that are intended to demonstrate that state-of-the-art thermal control systems are adequate to store cryogenic propellants in a deep-space environment, nonvented, for as long as 1200 days.

The main purpose of the propellant thermal control system for any space propulsion module is to control the transfer of heat to the propellant from the surrounding environment. If this is done effectively throughout the mission, the propellant losses, when and if venting is necessary, can be minimized. Using high-performance, deep-cryogenic propellants (hydrogen, oxygen, and fluorine) for long-duration interplanetary missions requires highly sophisticated thermal control systems.

Several studies have previously examined the thermal control requirements for cryogenic stages for outer planet orbiter-type missions (refs. 1 to 3). Although performed under varying ground rules, all of these studies have indicated the feasibility of storing cryogenic propellants for long times in a deep-space environment. The common theme among these studies is the use of multilayer insulation, low-conductivity tank supports, stage orientation, and shadow shields for the nonvented storage of hydrogen.

For a stage oriented to the Sun, using shadow shields can reduce radiation heat transfer to the propellants from the Sun or the vehicle payload to a very low quantity. Shadow shield system designs have been investigated analytically at the Lewis Research Center (refs. 4 to 6). In addition, experimental work (refs. 5 and 6) has confirmed the effectiveness of shadow shields on at least a model scale (i. e., as large as 1.2 m (4 ft) in diam). The satisfactory thermal performance obtained for the small-diameter shields further justified the use of full-scale shields (e. g., 3.0 m (10 ft) diam) for future cryogenic upper-stage application. Questions remained, however, regarding whether or not large-diameter shadow shields, capable of mechanically withstanding the anticipated thermally induced loads, could be successfully designed and fabricated.

A full-scale thermal model, designated the cryogenic storage test vehicle (CSTV), was fabricated and tested to demonstrate that a total heat leak into the liquid-hydrogen fuel tank of less than 0.2 watt (0.68 Btu/hr) could be achieved (ref. 7). Two full-scale, lightweight shadow shields were used as a part of the total thermal protection system on the model. This report documents the shadow shield design, fabrication, and installation procedures as well as the structural testing of a prototype shield.

Although test measurements were made in the U. S. customary system of units, the International System (SI) is included for reporting purposes.

## DESIGN

### General Requirements

The principle of shadow shield performance is illustrated in figure 1. The mode of heat transfer through a shield system is similar to that of multilayer insulation (i. e., radiation between highly reflective shields). However, because each shield surface has a finite view to space, a large fraction of the heat emitted by the hot source is radiated and/or reflected to space rather than to the cryogen. The heat transfer rate through a shadow shield system is a function of the number of shields, the shield emissivity, and the spacing between the heat source and the heat sink as documented in references 4 to 6. In general, increasing the number of shields and/or the spacing and decreasing the emittance will decrease the heat transfer rate.

Before the shadow shield system could be designed for the thermal test model of

reference 7, certain envelope, structural, and flight-load ground rules and assumptions had to be established. These were (1) space allocation for the shields, (2) anticipated shield operating temperatures, and (3) anticipated flight loads. Each of these, as well as other materials considerations, are discussed in the paragraphs that follow.

Shield size and space allocation. - Figure 2 is a sketch of the thermal test model of reference 7. The oxidizer tank, its supporting structure, and the engine are shown for completeness although only the liquid-hydrogen tank, its support structure, the shadow shields, and a simulated payload were part of the actual demonstration test package. The test package was designated the cryogenic storage test vehicle (CSTV). It can be seen that any space allocated for the shadow shields will increase the stage length. This in turn increases the stage mass and also the distance between the stage center of gravity and the engine thrust point. A design objective then was to provide a stage of minimum length consistent with meeting the shield system thermal goal. The weighting of these factors as well as others resulted in the configuration shown in figure 2. The upper shield (i. e., payload shield) is located 20.32 centimeters (8.0 in.) from the payload, and the lower shield (i. e., tank shield) is located 12.70 centimeters (5.0 in.) from the upper shield. A spacing of 1.27 centimeters (0.5 in.) exists between the lower shield and the top of the liquid-hydrogen-tank insulation.

The two shields selected were double-sheeted shields. For clarity, figure 3 sketches the double-sheeted-shield concept. The shield assembly consists of a hoop (or rim) with reflective sheets stretched across the bottom and top of the hoop to form the double-sheeted shield.

The spacing between the adjacent sheets should be as small as practical in order to result in a thin shield. For a fixed payload-to-tank spacing the thinner shields will allow more heat to escape into space. There is a limit, however, to how close the sheets of a shield assembly can be; that is, they must not touch and thereby thermally short.

The diameter of the shadow shield assembly should be only large enough to prevent any direct line of sight between the payload and the liquid-hydrogen tank. However, for the CSTV, an outside diameter larger than that of the payload was selected. This selection allowed for some error in the orientation of the vehicle while still preventing a direct line of sight between the propellant tank and the Sun.

Shield operating temperature. - The temperature extremes encountered by a vehicle during its mission are generally represented by the payload temperature (which is the warm extreme) and the liquid-hydrogen-tank temperature (which is the cold extreme). In an actual flight the shields will have an operating temperature somewhere in between these two values. However, the test conditions of the CSTV program were to be more severe than conditions anticipated during typical space flight because a null test had to be conducted to determine extraneous heat leaks into the test tank. Expected shield steady-state operating temperatures for the various CSTV test conditions were obtained from an existing analysis (ref. 6) and are shown in figure 4. A more-detailed discussion

of the cooldown transient period and the temperature differential stated for this period appear later in the section Thermal Analysis. The stresses and deflections induced in the shield components (i. e., sheets and rim) because of these imposed temperatures were regarded as design requirements that had to be met.

The initial test condition considered is that of the test vehicle exposed to vacuum with the surrounding temperature at 289 K (520° R). The next phase is the rapid chilling of the surrounding environment to 22 K (40° R). The temperatures shown for the transient cooldown occur at a point in the chilling process when the temperature differential between the shadow shield sheets and the shadow shield rim is at a maximum. The third phase, the null steady state, is begun when all parts of the test vehicle have come to a steady-state temperature of 22 K (40° R). The last test condition, the space phase, is representative of the conditions simulated during space testing. During this phase the payload is at 289 K (520° R) and the surrounding environment is at 22 K (40° R).

Flight loads. - If the shields were installed on an actual flight vehicle, they would be subject to dynamic loading through the various phases of the vehicle flight profile. These loads are due to vibration and acceleration caused by launching, staging, and in-space maneuvers of the vehicle. These loads cannot be defined precisely without an assigned launch vehicle. However, based on past experience, a 6-g loading appeared adequate for design of the shield structural members. This load was treated as static in the design of the shields.

Other considerations and materials selection. - The environments to which an actual space vehicle is exposed are extremely varied and may include high humidity prior to launch, high vacuum, temperature excursions caused by exposure to direct solar radiation, and meteoroid impact. The properties of the materials selected for a shield system should be able to withstand the effects of these environments. As we see it, the major properties to be considered are surface emissivity, durability, stability, fatigue resistance, and stress relaxation.

No specific in-house test program was conducted to rigorously evaluate candidate shield materials in all these environments. Instead, a survey was made of materials test data, taking advantage of already reported information as well as some being generated as part of other presently existing government programs (e. g., unpublished data from General Dynamics, Convair Division). Based on these sources and the known design requirements for this program, a reinforced double-aluminized Mylar material (Schjeldahl X-850) was selected for the shadow shield sheets and an aluminum alloy (6061-T6) was selected for the rim and its support brackets.

Another potential candidate for the shield material is a laminate of aluminized Kapton outer sheets attached to a fiberglass centerbody sheet. This composite would be more durable than the Schjeldahl X-850 during temperature excursions caused by exposure to direct solar radiation. The CSTV shadow shield assemblies, however, would only see 289 K (520° R) as an upper limit during this test program. Therefore, because

of the immediate availability of test data on Schjeldahl X-850, as well as the increased cost of the aluminized Kapton/fiberglass composite, the Schjeldahl X-850 material was used.

### Discussion of Materials

Sheet material. - Schjeldahl X-850 is a  $0.0078\text{-g/cm}^2$  ( $0.016\text{-lb/ft}^2$ ) laminate of two sheets of single-aluminized Mylar with a Dacron-reinforced netting sandwiched in between. Unreinforced aluminized Mylar has been thermally tested in the past (refs. 5 and 6) for use as shadow shield sheets. It was found that the surface and physical properties of the aluminized Mylar were excellent for this type of application. The center-located Dacron netting of the Schjeldahl X-850 provides a rip-stop feature and a ruggedness to the laminate that unreinforced aluminized Mylar does not have. The X-850 material is presently being used as side-wall radiation barriers on an improved version of the Centaur upper-stage vehicle.

Additional tensile and creep screening tests on the X-850 material were run at Lewis. Since the material was manufactured in rolls, testing was conducted on samples that had their long axis parallel to the roll direction as well as on samples that had their long axis normal to the roll direction (i. e., cross-roll direction). The results of these tests are shown in figures 5 and 6. Figure 5 shows the load-strain relation obtained for tests conducted both at room temperature and at liquid-nitrogen temperature. The end points of each curve correspond to the loads at which specimen failure occurred. Figure 6 shows the results of room-temperature creep tests conducted at two different load conditions. These data were obtained in order to resolve a design consideration discussed later in this report. Significant creep was noted for the  $8.8\text{-N/cm}$  ( $5\text{-lb/in}$ ) load during the early part of the test for the cross-roll sample only. After about 200 hours, however, the rate of elongation diminished. At a loading of  $4.4\text{ N/cm}$  ( $2.5\text{ lb/in}$ ) the creep rate was not considered to be large for either sample.

Rim and bracket material. - High temperature stresses could be developed in the shield sheet material as a result of improper selection of the rim material. Two materials in common usage for spacecraft are aluminum alloys and stainless-steel alloys. Figure 7 compares the thermal contraction of X-850 with that of 6061-T6 aluminum and 304L stainless steel. The data for the metals were obtained from reference 8; and those for the Schjeldahl X-850 are unpublished data from General Dynamics, Convair Division. To minimize thermal strain in the X-850 shield material, 6061-T6 aluminum was chosen for the rim since its thermal contraction provided a better match to the X-850 than did the 304L stainless steel. To avoid further problems with materials of different thermal contraction, 6061-T6 aluminum was also used for the shield support brackets.

One concern with using aluminum for both the shield rim and the support brackets was its high thermal conductivity. For the CSTV program there was concern that a large amount of heat would be conducted from the shield to the vehicle structure and thence to the cryogenic propellant tank. This concern can be dispelled since bolted joints between the shield brackets and the vehicle structure could provide a thermal contact resistance. If larger resistances were required, additional thermal blockage could be installed at these points.

### Thermal Analysis

Besides the steady-state operating temperatures, the mechanical design of the shadow shield assembly required knowing the extremes of the temperature difference between the X-850 sheets and the shield rim in order to determine the level of thermally induced stresses. Since the rim was the heavier cross section and is the most massive of the two shield components, it would cool much more slowly than the X-850 sheets. This thermal lag could cause a large transient tensile stress in the sheets.

To approximate the temperature differential that can exist between the rim and the sheets, a simple transient heat transfer equation relating heat capacity to thermal radiation heat loss can be used. The equation may be written as

$$M_x c_{p,x} \frac{dT_x}{d\theta} = \alpha \epsilon_x A_x (T_{\text{sink}}^4 - T_x^4) \quad (1)$$

(See appendix A for definitions of the symbols.) The subscript  $x$  refers to either the rim or the shield sheet, whichever is being considered. For a reflective sheet the area term is represented by only one surface of one of the sheets; for the shield rim the entire surface area is used. The rim loading produced by the thermal contraction of the shield sheets can be obtained by using, in conjunction with figures 7 and 5, the temperature histories of each of the two components. Since equation (1) imposes a step change in the component being considered, it will necessarily predict histories of decreasing temperatures that are extremely steep. The conditions of both the test program and an actual launch would result in transient chilldowns much slower than that assumed by equation (1).

The solution of equation (1) for an initial temperature of 289 K (520° R) and a constant sink temperature of 22 K (40° R) is shown in figure 8. A working plot of the tensile load on the sheets was made by using the temperature histories of figure 8, the thermal contraction data of figure 7, and the liquid-nitrogen load-strain curve of figure 5. The maximum tensile load was found to occur at 24 minutes; and the maximum



temperature differential at 18 minutes into the cooldown.

Table I compares the thermally induced forces in the shield caused (1) by temperature differences from this transient cooldown design analysis, (2) by expected CSTV null test conditions, and (3) by the CSTV preliminary steady-state operating temperatures previously discussed in the section Shield operating temperature. The conclusion is easily drawn that the transient cooldown design condition is more critical than any of the steady-state conditions that would be encountered during CSTV testing or during an actual flight.

Table I also shows that during steady state the sheet temperatures are equal to or higher than the rim temperatures. This temperature difference suggests that the sheets may loosen if they are not properly pretensioned during installation. Also, under steady-state space conditions, the payload shield sheet temperatures disclose that the top sheet would loosen more than the bottom sheet. If the two sheets could be connected, it would be easier to balance these movements, relative to the rim, over both sheets.

Note again that all the steady-state and transient temperatures discussed so far were considered preliminary and only as input for mechanical design purposes.

### Mechanical Design

The mechanical design effort was performed to provide a shield system that would meet the structural and thermal loads imposed. A structural load of 6 g's in the direction of the stage axis was considered in addition to all the thermal conditions of table I. The design is discussed separately for the sheets, the rim, and the rim supports.

Sheet pretension. - The fact that some minimum pretension is required to keep the sheets from touching each other can be seen in test phase 3 (payload shield) of table I. When the shield assembly is at these temperatures, there are essentially no tension forces keeping the sheets of the assembly apart.

To establish a relation between sheet tension and sheet deflection, a calculation model was hypothesized that consisted of a unit width (2.54 cm (1.0 in.)) of shield sheet material whose weight was suspended from its two end points. The following one-dimensional equations from reference 9 were used to quantize the relations desired:

$$Y_{ss} = \frac{H_{ss}}{w_o} \left[ \cosh \left( \frac{w_o R_{ss}}{H_{ss}} \right) - 1 \right] \quad (2)$$

$$K_{ss} = H_{ss} \cosh \frac{w_o R_{ss}}{H_{ss}} \quad (3)$$

If  $H_{ss} \gg w_o R_{ss}$  and, further, equation (3) is substituted into equation (2),

$$Y_{ss} = \frac{K_{ss}}{w_o} \left[ \cosh \left( \frac{w_o R_{ss}}{K_{ss}} \right) - 1 \right] \quad (4)$$

A minimum value of pretension required to separate the top and bottom sheets can be calculated by assuming that the lower sheet of the assembly remains flat and that the top sheet is allowed to deflect such that it just contacts the lower sheet. For this assumption and a distance of 3.8 centimeters (1.5 in.) between the sheets, equation (4) yields a  $K_{ss}$  of 0.224 N/cm (0.128 lb/in). Hence, only a small amount of pretension is necessary to keep the shield sheets from touching. Considering for a moment an upper value for sheet tension, a conservative limit can be obtained from the creep tests discussed previously (i. e., fig. 6). The conclusion that can be drawn from this figure is that an acceptably low creep results from a total tension value of 4.38 N/cm (2.5 lb/in). Further, using equation (4), the 4.38-N/cm (2.5-lb/in) loading confines sheet deflection to 0.196 centimeter (0.077 in.).

Based on these limits, we decided to put only a slight amount of pretensioning into the shield sheets. The amount of pretensioning employed was sufficient only to prevent excessive visible sagging of the sheets (i. e., greater than approximately 0.64 cm (1/4 in.)). According to equation (4) the deflection of 0.64 centimeter (1/4 in.) corresponds to a force of only 1.34 N/cm (0.766 lb/in).

Sheet-to-rim connection. - The top and bottom sheets of each shield assembly were fastened together around the rim. This was done so that the forces created by differential thermal contraction could be equalized between the two sheets without causing large torsional forces in the rim. To fasten these sheets around the rim, 30 equally spaced tabs (3.81 cm (1.5 in.) wide) were installed on each sheet (fig. 9). The criterion for selecting the number of tabs was based on providing only enough tension (accounting also for the thermal forces) (1) to prevent excessive sagging of the sheets, (2) to transfer a minimum loading to the rim, and (3) to accommodate random tab failures. Each tab was adhesively bonded to the sheet surface and then stitched to it to provide further assurance of joint integrity. Prior to use, this attachment method was developed on small test samples that were tensionally loaded with 89 newtons or 23.3 newtons per centimeter (20 lb or 13.3 lb/in) for several days at both ambient and liquid-nitrogen temperatures. No failures or joint deterioration occurred during this development work.

The tensile forces that were developed because of the thermal contraction of the sheets relative to the rim have, up to this point, been considered to produce a uniform circumferential loading in the rim. With the introduction of tabs, more of a point loading of the rim will be taking place. The relations among uniform loading  $w_{ur}$ , pure point loading of the rim at any given set of opposing sheet tabs  $W$ , and the load per unit

width of a single sheet tab  $w_t$  are as follows:

$$W = \frac{\pi D_{ss}}{30} w_{ur} \quad (5)$$

$$w_t = \frac{\pi D_{ss}}{(30)(2)(\text{Tab width})} = \frac{\pi D_{ss}}{90} w_{ur} \quad (6)$$

These equations may easily be derived from the definitions, the physical measurements of the variables, the number of sheet tab pairs, and the diameter of the shield sheet.

Equation (6) can be used to compare the design loads of table I with the tensile load data of figure 5 in order to determine the integrity of the sheet tab material under the proposed design test phases. For the design loadings ( $w_{ur}/2$ ) in table I and from equation (6), the load per unit width of a shield support tab  $w_t$  is 109, 80.4, and 68.9 N/cm (62.3, 45.9, and 39.4 lb/in) for the cooldown transient, null, and space steady-state test phases, respectively. The value for the space steady-state phase is below the failure data shown in figure 5 for the sheet material. The loads per unit width for the transient cooldown and null phases, on the other hand, are above the failure data. However, the shield sheet tabs were joined over the rim by a nonrigid wire clip connection device (fig. 9) and, further, some sheet creep could be expected that would result in a certain amount of stress relaxation. Thus, not all of the calculated tensile loading force would be present in the actual hardware. The reader should also remember that the design condition that gave rise to the 26.6-N/cm (15.2-lb/in) cooldown transient tensile loading is much more severe than the condition that would be present during an actual launch. Also, the second design test phase (i. e., null) is an extreme environment not encountered in a space flight profile. The design therefore proceeded but under the full recognition that the sheet-to-rim connections appear structurally marginal as a result of the mechanical design analysis employed.

The initial pretensioning of 1.34 newtons per centimeter of tab width (0.766 lb/in) is additive to the above tensile forces. It, however, is very small when compared with the other tensile forces present during the transient cooldown and the null condition and was therefore neglected.

Rim. - The rim used to support the shadow shield sheets should be an optimization of both structural strength and minimum weight. The loads imposed by the sheets result generally in compressive stresses in the rim. Therefore, the design concentrated on the prevention of buckling instability.

The results of the rim design considerations are presented in appendix B. From this work it was concluded that a 3.8-centimeter-outside-diameter (1.5-in. -o. d.), 0.165 centimeter-diameter-wall (0.065-in. -wall) tubular design would meet the struc-

tural requirements while still providing a lightweight structure.

Shield support brackets. - The brackets were used to support the shield assembly from the vehicle structure struts. Any radial movement due to thermal contraction of the shield rim and vehicle struts could be accounted for by designing the brackets as springs permitting radial movement. A total of six brackets were required per shield; one bracket was bolted onto each of the six pairs of struts.

Appendix C contains the calculations, which showed that 0.24-centimeter (3/32 in.) by 2.5-centimeter (1-in.) aluminum strap would be sufficient to support the shield weight. Figure 10 shows one of the six brackets mounted on the inner surface of the shield rim.

## FABRICATION AND ASSEMBLY

With the exception of the shield sheets, all the parts of a shield assembly can be fabricated in a sheet metal shop. The manufacture of the metal parts is not described in this report. However, fabrication of the X-850 shield sheets and their assembly into a completed shield did require special effort and is discussed in the following sections.

### Sheet Fabrication

The X-850 material used for the shield sheets was commercially available only in rolls 1.17 meters (46 in.) wide. This made it necessary to use three separate pieces of material to fabricate each circular sheet. The separate pieces composing each sheet were first butted side by side. Surfaces of adjacent pieces of material were visually matched for smoothness. The junction between two adjoining pieces was then covered by adhesively bonding on a continuous strip of X-850 material 5.1 centimeters (2 in.) wide. The joined pieces were then turned over and a second continuous cover strip was bonded over the junction on the reverse surface of the partial assembly to complete the joint.

When each cover strip was bonded on the sheet seam, air bubbles were sometimes trapped between the cover strip and the shield pieces. These were removed by applying pressure with a small roller immediately after the adhesive-coated surfaces had been brought into contact with one another. Each glued joint was allowed to set under pressure for 48 hours.

After the tabs were bonded and stitched to the sheet edge, a series of weights were suspended on the tabs to stretch the sheet over the rim (fig. 11).

The adhesive used in all bonding operations was Goodyear's Pliobond 4001/4004 polyester resin system. For this application, where the two-part adhesive was to be applied to the surfaces by brushing, it was mixed at a weight ratio of 100 parts of resin

to 4 parts of hardener.

This attachment technique was used to make small-scale samples prior to using it for full-scale shadow shield joints. The small-scale samples were tested under simulated loading conditions. The results of these tests were used to determine the proper drying time, adhesive thickness, and bonding pressures for the full-scale joints.

### Shield Assembly

After the sheets had been stretched over the rim, fastening was completed by connecting the tabs from opposing sheets over the outside surface of the rim with wire clips that were pretensioned by means of a bolt assembly (fig. 9). To pretension the sheet evenly, it was necessary to fasten a set of opposing tabs simultaneously at two different positions diametrically opposite each other on the rim.

The finished shield assembly was a very light structure having a total weight of only 8.3 kilograms (18.2 lb). A weight breakdown of a shield assembly appears in table II.

### Shield Installation

When installing the shield assemblies into the structure of the CSTV, it was necessary to release a number of the tabs on the shield rim to allow the shield sheets to be temporarily folded back (fig. 10). After the shield assembly had been lowered to its proper position and the shield support brackets fastened to the CSTV structure, T-shaped slits were cut from the outer edge of each sheet to each set of structure penetration holes to allow the sheets to be fitted around the structural members. Later, these slits were taped closed and annular collars (fig. 9) were fitted around the structure struts to block radiation through any gap remaining between the sheet and the strut. In addition, one extra tab was added to each sheet for every pair of structure holes in order to support the sheet where it had been cut. In total, six additional tabs were added per sheet.

This description deals with the two shields constructed for use on the CSTV. The prototype shield differed from them only in the fact that slits did not have to be cut in this shield to allow mounting on its strut simulators.

## TEST PACKAGE

### General

The test package constructed to determine the structural integrity of the prototype

shield consisted of a shield assembly and a payload simulator mounted inside a 3.96-meter-diameter (13-ft-diam), liquid-hydrogen-cooled shroud. The shroud was suspended inside a 7.62-meter-diameter (25-ft-diam) vacuum chamber. A schematic of the major components is given in figure 12.

The tests for the prototype shield were planned to evaluate the stress as well as any shield sagging during three separate conditions: (1) short-term transient cooldown; (2) long-term, steady-state exposure; and (3) induced warmup of the assembly following steady-state exposure. These test environments were simulated by the shroud and payload cooldown, shroud and payload steady state, and payload warmup.

### Shadow Shield Assembly

Figure 13 shows the prototype shield mounted beneath the payload simulator and the lid of the shroud. A circular ring (referred to as a handling ring) of lightweight pipe was used as the transition piece between the shield assembly and the payload simulator. Vehicle structure strut simulators were an integral part of the handling ring. They served not only as mounting tubes for the shield support brackets, but also as hard points from which to mount the lighting and television equipment required during testing. The handling ring was suspended at six points from the payload simulator by using loose pin joint linkage.

### Payload Simulator

The payload simulator consisted of a 3.05-meter-diameter (10-ft-diam), 0.64-centimeter-thick (1/4-in. -thick) aluminum plate bolted directly to a 10-centimeter (4-in.) rolled channel ring. On the back (or top) side of the simulator, 2.5-centimeter-inside-diameter (1-in. i. d.), D-shaped, liquid-hydrogen flow tubes were welded to enable cooling of the simulator to 22 K (40° R). Electrical resistance heater pads were adhesively bonded to the bottom surface of the 0.64-centimeter (1/4-in.) body plate of the simulator. These units allowed controlled heating of the simulator after a cold-flow test period. These heater strips were in turn covered by adhesively bonding on a 0.16-centimeter-thick (1/16-in. -thick) aluminum faceplate.

### Shroud and Vacuum Chamber

During part of the test program a requirement existed that the prototype shield see a surrounding temperature of approximately 22 K (40° R). As a result, the shield-payload

combination was mounted within a shroud nominally 3.96 meters (13 ft) high and approximately 3.96 meters (13 ft) in diameter. The shroud is shown mounted inside the vacuum chamber in figure 14. The vertical body of the shroud was composed of 12 rectangular panels with vertical, D-shaped, liquid-hydrogen flow tubes of 2.5-centimeter (1-in.) inside diameter welded on the outside surfaces. One of the vertical panels was a door, which allowed access to the shroud interior to facilitate repair of any test configuration malfunctions. Both the bottom and the top of the shroud were flat and also had liquid-hydrogen flow tubes mounted on their exteriors. The fourth major part of the shroud assembly was a group of three annular baffles also capable of being cooled with liquid hydrogen. The baffles were needed for thermal isolation of the CSTV of reference 7 and were not a required piece of hardware for this test. Each major subsystem of the shroud (i. e., vertical walls, bottom, top, and baffles) had resistance heaters adhesively bonded between the liquid-hydrogen flow tubes to allow heating of the surfaces to room temperature. The inside surfaces of the walls, the bottom, and the top, as well as the top surfaces of each baffle, had a covering of 0.95-centimeter (3/8-in.) hexagonal honeycomb that was 0.95 centimeter (3/8 in.) thick. These honeycombed surfaces were also sprayed with 3M Black Velvet paint.

All thermal testing of the prototype shield was done in a 7.62-meter-diameter (25-ft-diam), spherical, side-loading vacuum chamber. The entrance door to the chamber had a diameter of 6.1 meters (20 ft). The "clean-dry-empty" vacuum capability was approximately  $1.07 \times 10^{-4}$  N/m<sup>2</sup> ( $8 \times 10^{-7}$  torr).

## INSTRUMENTATION

Instrumentation on the prototype shield assembly was designed to detect sheet sag, sheet and rim temperatures, and rim deformation due to temperature-induced loads. Figure 15 is a sketch of the instrumentation arrangement on the shield assembly.

Two different electrical circuits (figs. 15(a) and (b)) were used to check for excessive sagging of the shield sheets. One circuit was connected to lightweight contacts located at the center of each of the inward-facing surfaces of the two sheets. This circuit was used to determine whether or not the two sheets touched each other at any time during testing. The second circuit consisted of a diametrically stretched wire located 3.18 centimeters ( $1\frac{1}{4}$  in.) below the face of the lower shield surface. One support post of this wire is visible in figure 9. This circuit was used to detect excessive sag of the bottom shield sheet.

Temperatures of the sheets and the rim were monitored at eight locations: two positions on the rim and three positions on each of the two shield sheets (fig. 15(c)). All these temperature transducers were 0.25-millimeter (10-mil) Chromel-constantan thermocouples referenced to a 78 K (140° R) electronic oven. The sensors located on

the shield sheets were mounted by first laying a strip of double-adhesive-backed Mylar tape (2.5 cm (1 in.) wide) along a 0.61-meter (2-ft) isothermal path desired for the wires. The thermocouple and its lead wires were then laid on the exposed tape surface, and the assembly was covered with aluminized Mylar tape. Thermocouples on the rim were adhesively bonded at their measurement junction, and their lead wires were spot glued to the rim over a minimum distance of 0.61 meter (2 ft).

Strain gages (fig. 15(d)) were applied only to the shield rim to monitor any potential onset of buckling due to thermally induced loading. Fourteen active gages, all installed with temperature-compensating gages, were positioned over one-third of the rim circumference. All gages were attached by adhesive bonding. These strain gages were installed both in the rim plane and normal to it before any loading was applied to the rim by tensioning of the shield sheets. It was anticipated that, should rim buckling become imminent, the strain gages would register either erratic and/or large-magnitude readings well beyond those imposed by the tensioning of the shield sheets.

A television package (fig. 15(e)) was suspended beneath the section of test package that was instrumented with thermocouples and strain gages. The package consisted of a camera with a wide-angle lens, incandescent lights, and a light reflector plate. Mirrors mounted from the shield handling ring were used to obtain a reflected view of the flatness of the bottom shield sheet. The housing containing the television camera was purged with inert gas and was also heated. Due to the reflectivity of the shield surfaces, an indirect lighting technique was employed to illuminate the bottom sheet of the shield. Lights were mounted facing the reflector plate, which was coated with flat white paint. In addition to the television monitor in the control room, a video tape recorder was used to record any unforeseen events.

The temperature of the payload simulator was monitored in six places by means of platinum resistance temperature sensors adhesively bonded to its bottom face plate. Shroud surface temperatures were measured by a combination of platinum resistance sensors and 0.51-millimeter (20-mil) Chromel-constantan thermocouples. These transducers were adhesively bonded to the outside surfaces of the shroud components.

Measurements were recorded on an automatic voltage digitizing system and/or continuous direct-reading strip charts. Digitized data were recorded only periodically, depending on whether the test hardware was going through a transient or a steady-state condition. During transients, digitized data recordings were taken as frequently as every 2 minutes. During a steady-state period they were taken at least every 10 minutes.

## PROCEDURE

The experimental test period can be divided into three main sections: (1) shroud



and payload simulator cooldown, (2) shroud and payload steady-state exposure at 22 K (40° R), and (3) a payload warmup transient.

Following test hardware instrumentation checkout at ambient pressure and temperature the chamber was closed and evacuated to the low  $1\text{-N/m}^2$  ( $10^{-2}$ -torr) range to allow for outgassing of the shield assembly. After the hydrogen flow system was leak checked, the chamber was pumped down to the low  $10^{-3}\text{-N/m}^2$  ( $10^{-5}$ -torr) level.

Phase 1 of the test procedure was started by initiating a flow of liquid hydrogen from the storage dewar through the warm transfer plumbing to the payload simulator and all four circuits of the shroud simultaneously. During initial cooling, hydrogen flow to the shroud and the payload simulator was regulated by remotely controlled valves immediately upstream of the test hardware. After cooling of the simulator and shroud surfaces had started, liquid-hydrogen flow control was regulated by two-position demand valves downstream of both the simulator and each of the four circuits of the shroud. As the shroud cooled down, thermal strains in the shield rim were monitored. Temperature differentials between the sheets and the rim were carefully watched.

Phase 2 (shroud and payload steady-state operation) of the test procedure was realized after completion of hardware cooling. This period lasted for 9 hours, during which temperatures and strains were continuously monitored.

Phase 3 consisted of terminating liquid-hydrogen flow to the payload simulator and then warming it successively to each of three different temperature levels in order to obtain data on sheet sag.

Television was used periodically during all test phases to view the shield assembly. The total number of visual observation periods (17), as well as the duration of each period ( $<10$  sec), was closely regulated so as not to influence the temperatures of the shield assembly by the addition of heat from the television package.

## RESULTS AND DISCUSSION

The three test phases of cooldown, steady state, and payload warmup were conducted consecutively without interruption. Notwithstanding a partial failure of the payload simulator faceplate, which resulted in a lower-than-anticipated loading on the shield assembly during the transient period only, the structural utility of the shield assembly was demonstrated.

Figure 16 is a plot of the temperatures of the shroud and payload simulator as functions of time. Also spotted on the figure are the test phases that will be discussed. Figure 17 is a plot of shield and rim temperatures over the same time base. The average payload temperature has been added to the plot for reference.

The rim loading  $w_{ur}$  produced during the test period was calculated by using the temperature histories of the rim and the shield sheets as well as the thermal contraction

and short-time load data in figures 5 and 7. Any rim loading reduction that might have occurred because of the nonrigid wire clip assemblies connecting opposing sheet tabs was neglected. The technique of calculating  $w_{ur}$  was the same as that employed earlier in the section Thermal Analysis. The resulting load history is plotted in figure 18.

Equations (B11) to (B14) relate the in-plane stress at the inner and outer surfaces of the shield rim, both at and between the sheet tab locations, to the point loading  $W$  imposed by each pair of opposing sheet tabs. From Hookes' law (i. e.,  $E_r = \sigma/\tau$ ) and equation (5), equations (B11) to (B14) can be rewritten as follows in terms of the strain  $\tau$  and the uniform rim loading  $w_{ur}$ :

(1) For the inner surface of the rim at load points

$$\left. \begin{aligned} \tau &= \frac{\pi D_{ss} w_{ur}}{30 E_r} (-0.742) = w_{ur} (-3.060 \times 10^{-6}) \quad (\text{SI units}) \\ \tau &= \frac{\pi D_{ss} w_{ur}}{30 E_r} (-4.791) = w_{ur} (-5.359 \times 10^{-6}) \quad (\text{U. S. customary units}) \end{aligned} \right\} \quad (7)$$

(2) For the outer surface at load points

$$\left. \begin{aligned} \tau &= \frac{\pi D_{ss} w_{ur}}{30 E_r} (5.792) = w_{ur} (2.388 \times 10^{-5}) \quad (\text{SI units}) \\ \tau &= \frac{\pi D_{ss} w_{ur}}{30 E_r} (37.374) = w_{ur} (4.181 \times 10^{-5}) \quad (\text{U. S. customary units}) \end{aligned} \right\} \quad (8)$$

(3) For the inner surface between load points

$$\left. \begin{aligned} \tau &= \frac{\pi D_{ss} w_{ur}}{30 E_r} (4.174) = w_{ur} (1.721 \times 10^{-5}) \quad (\text{SI units}) \\ \tau &= \frac{\pi D_{ss} w_{ur}}{30 E_r} (26.932) = w_{ur} (3.013 \times 10^{-5}) \quad (\text{U. S. customary units}) \end{aligned} \right\} \quad (9)$$

(4) For the outer surface between load points

$$\left. \begin{aligned} \tau &= \frac{\pi D_{ss} w_{ur}}{30 E_r} (0.904) = w_{ur} (3.727 \times 10^{-6}) \quad (\text{SI units}) \\ \tau &= \frac{\pi D_{ss} w_{ur}}{30 E_r} (5.831) = w_{ur} (6.522 \times 10^{-6}) \quad (\text{U.S. customary units}) \end{aligned} \right\} \quad (10)$$

Positive values of strain  $\tau$  denote tension; negative values denote compression.

By using these equations and the load history shown in figure 18, a strain history based on the actual temperature surroundings imposed on the sample shield during the entire test period can be calculated. These calculated strain histories will be compared to experimentally measured strain values from gages 1 to 8 (see fig. 15) in order to show that the simplified mechanical and thermal analyses used in the shield design are sufficient to produce a lightweight, rugged product that will maintain its structural integrity.

The out-of-plane strain gages (i. e., gages 9 to 14 (fig. 15)) were used only to detect a complete failure of the rim. Since no failure occurred, these gages are not discussed further.

#### Structural Performance during Cooldown

This interval constituted the first 33 hours of the entire test period. All surfaces of the shroud were cooled to liquid-hydrogen temperature levels within 3.8 hours after testing started. The payload simulator temperature, however, lagged significantly behind (fig. 16) due to rupture of the adhesive bond between its faceplate and the liquid-hydrogen-cooled backplate. Television observation of the shield during this test interval verified that all tabs and sheet seams within the viewing field remained tight.

The shield assembly was designed by assuming that the shroud and the payload simulator cooled instantaneously to 22 K (40° R). Actually, the thermal lag of the shroud was approximately 4 hours and that of the payload simulator much longer. These time lags substantially reduced the cooling rate of the shield sheets and the rim. During the test interval the maximum differential between the rim temperature and an average sheet temperature (i. e.,  $\Delta T_{str} = T_3 - (T_{12} + T_1)/2$ ) was only 32.8 kelvins (59 deg R) instead of the design value of 96 kelvins (173 deg R). From this standpoint the imposed surrounding temperature was not severe enough to test the shield assembly to its cooldown design value (table I, phase 1). However, as has been pointed out, the design limit was much more severe than the conditions that would be present during an actual launch.

Figure 19 details the comparison between the calculated strain histories (based on

experimentally measured sheet and rim temperatures) and the readings from strain gages 1 to 8. The comparison is made both at and between tab loading points. As was noted in the section Shield Assembly, one extra tab was added to each sheet for every pair of structure holes cut in the sheet material. Strain gage combinations 1 and 2 and 7 and 8 were located in the immediate vicinity of these structure holes (fig. 15) and were treated as indicating strain information occurring at a load point. Strain gages 5 and 6 were mounted directly at a load point. The remaining gage pair (i. e., 3 and 4) was used to indicate rim strain between the tab loading locations.

From only the cooldown interval (the first 33 hr) in figure 19, it can be seen that the experimentally measured strains are in a region that implies a lower rim loading than predicted by using the simplified design analysis. This fact is true for all data except those taken during a short period shown in figure 19(a). This single exception was not considered significant since the absolute level of the strain values for this short period was quite small and hence does not affect the overall observation that the simplified design analysis is conservative.

A second observation that can be alluded to from these figures is that the shield rim was not symmetrically loaded during cooldown. This fact is evident from comparisons of strain histories from gages 1 and 7 as well as from gages 2 and 8. These data suggest that the thermally induced loading could be better distributed if necessary by improving the sliding contact between the sheet tabs and the shield rim.

As mentioned earlier, this cooldown section of the test did not produce the thermal strains that had been used in the design phase. However, since the experimentally measured strains indicate a very conservative design, it is our opinion that if the shield assembly had been exposed to a surrounding as severe as that used in the design phase, the shield still would have maintained its integrity.

Lastly, this test interval also verified that no structural problems would exist during the test phases planned for the two shadow shields built for the CSTV program.

### Strains During Steady State

This second interval of the test period was 9 hours in duration. The cooldown rate of both the rim and the shield sheets was less than 1 kelvin/hr (1.8 deg R/hr), and the temperature difference between the rim and the sheets  $\Delta T_{str}$  averaged out at 20.6 kelvins (37 deg R). Because the sheet-to-rim temperature differential was maintained almost constant, this test interval provided a good opportunity for the shield sheet material to creep. The television camera and lights were turned on several times during this test period. The observation periods were spaced sufficiently apart to avoid upsetting the thermal balance between the shield sheets and the shield rim. During all observations the tabs and the sheet seam in the view field were found to be secure, and the

shield condition still remained good.

Consider now the calculated and measured rim strains during this steady-state interval (fig. 19). As in the cooldown period, the experimentally measured strains revealed that a lower loading was present than would be calculated by using the experimental temperature histories and the simplified design analysis.

The calculated loading  $w_{ur}$  produced in the rim for this test interval (fig. 18) was (1) greater than the design steady-state space loading shown as phase 3 in table I, and (2) almost 91 percent of the design loading considered for the null condition shown as phase 2 in table I. Since the experimentally measured strains plotted in figure 19 still indicate a conservative design, the authors concluded that no structural problems would exist during either the null test or the space steady-state phase of the CSTV program.

#### Thermally Induced Loading during Payload Simulator Warmup

This interval constituted the last 12 hours of the testing period. The payload simulator was warmed to three different temperature plateaus of 154, 204, and 264.4 K (277°, 367°, and 476° R). This testing was conducted to evaluate whether or not the shield sheets would sag to the point of touching as their temperature rose to above that of the rim.

The largest sheet-to-rim temperature differential was 49.4 kelvins (89 deg R) and was obtained just before the rim temperature reacted to the highest payload simulator heater setting. More frequent television observations of the test hardware were made during this test interval. No changes in the shield appearance were noted during the first two temperature plateaus. During the last heating step, some small wavy wrinkles normal to the bottom sheet seam appeared within the viewing area. Since no signals were observed in either of the electrical circuits, excessive sheet sag did not occur and hence the slight pretensioning in the shield sheets was concluded to be sufficient to prevent sheet contact.

Figure 19 also displays the calculated and measured rim strains during the warmup interval. Considering the comparisons, it can again be stated that, as in the cooldown period, the experimentally measured strains are generally in a region that implies a lower loading than would be calculated by using the simplified design analysis. The data in figures 19(a) and (b) that are an exception to this statement were not considered significant since the absolute level of the strain values for these short periods was quite small and hence does not affect the overall observation.

## Post-Test Inspection and Disassembly

When the prototype shield was removed from the shroud, a rough measurement of the sheet sag was conducted. For the top sheet of the shield assembly the central location of the sheet surface was 0.95 to 1.3 centimeters ( $3/8$  to  $1/2$  in.) below the horizontal plane of the rim. This amount of sag was at most 0.3 centimeter ( $1/8$  in.) more than the pretest condition. The center of the bottom sheet was still 2.5 centimeters (1 in.) above the electrical circuit wire. No difference between this measurement and the pretest condition could be found. The wrinkles on the bottom sheet were about 0.24 centimeter ( $3/32$  in.) deep and did not appear to be causing any loss of pretension in the tabs parallel to the sheet seams. All tab wires still appeared to be in tension.

The adhesively bonded tabs and sheet seams were also examined. No failures of the adhesive bonds could be found. The reinforcing stitchwork on some of the tabs was purposely removed. No peeling of these tabs at the glue joint was observed. The electrical circuits were rechecked; both were functioning normally. Finally, the shield sheets were removed from the rim. The removed sheets were remeasured with their fabricating template. The dimensions were found to be unchanged. The strain gage readings were taken before the tab wires were cut. All gages had returned to their original pretest values. This fact is significant. It implies (1) that all gages had been functioning and had registered only thermal strains during the test as planned and (2) that there was no appreciable loss of pretension in the tabs.

## CONCLUDING REMARKS

A 3.05-meter-diameter (10-ft-diam), full-scale, lightweight, double-sheeted shadow shield was designed as a deep-space thermal protection device for liquid-hydrogen propellant tankage. Both mechanical and thermal environmental requirements dictated the final design. A prototype shield assembly was fabricated and structurally tested through cooldown; steady-state low-temperature exposure; and transient warmup.

The results of the tests demonstrated that the simplified mechanical and thermal analyses used in the shield design are sufficient to produce a lightweight, rugged product that is structurally adequate for its intended application. The design concept appears simple, practical, and reliable. The thermal performance of the shield, when used as part of a complete insulation system, has been documented elsewhere and shown to be satisfactory.

To date, no other full-size, lightweight shadow shield has been built for thermal con-

trol in a deep-space environment. This program demonstrated that such a system could be made for use in future space exploration vehicles.

Lewis Research Center,  
National Aeronautics and Space Administration,  
Cleveland, Ohio, September 15, 1976,  
506-21.

## APPENDIX A

### SYMBOLS

A	area, $\text{cm}^2$ ( $\text{in}^2$ )
C	moment, $\text{cm}\cdot\text{N}$ ( $\text{in}\cdot\text{lb}$ )
$c_p$	specific heat at constant pressure, $\text{W}\cdot\text{hr}/\text{kg}\cdot\text{K}$ ( $\text{Btu}/\text{lb}\cdot^\circ\text{R}$ )
D	diameter, $\text{cm}$ ( $\text{in.}$ )
d	diameter, $\text{cm}$ ( $\text{in.}$ )
E	Young's modulus, $\text{N}/\text{cm}^2$ ( $\text{psi}$ )
F	force, $\text{N}$ ( $\text{lb}$ )
H	horizontal component of tensile force, $\text{N}$ ( $\text{lb}$ )
h	height, $\text{cm}$ ( $\text{in.}$ )
I	moment of inertia, $\text{cm}^4$ ( $\text{in}^4$ )
K	tensile force in a 2.54-cm- (1-in.-) wide strip of sheet material, $\text{N}$ ( $\text{lb}$ )
$l$	length, $\text{cm}$ ( $\text{in.}$ )
M	mass, $\text{kg}$ ( $\text{lb}$ )
R	radius, $\text{cm}$ ( $\text{in.}$ )
T	temperature, $\text{K}$ ( $^\circ\text{R}$ )
t	thickness, $\text{cm}$ ( $\text{in.}$ )
W	point load on rim at a tab pair location, $\text{N}$ ( $\text{lb}$ )
w	load per unit length, $\text{N}/\text{cm}$ ( $\text{lb}/\text{in}$ )
$w_o$	shield sheet mass per unit length for a 2.54-cm- (1-in.-) wide strip, $\text{N}/\text{cm}$ ( $\text{lb}/\text{in}$ )
$w_t$	load per unit width of a single sheet tab, $\text{N}/\text{cm}$ ( $\text{lb}/\text{in}$ )
$w_{ur}$	uniform loading per circumferential unit length of rim, $\text{N}/\text{cm}$ ( $\text{lb}/\text{in}$ )
x	angle such that $0 \leq x \leq \varphi$
Y	deflection, $\text{cm}$ ( $\text{in.}$ )
$\alpha$	Stefan-Boltzmann constant, $\text{W}/\text{cm}^2\cdot\text{K}^4$ ( $\text{Btu}/\text{hr}\cdot\text{in}^2\cdot^\circ\text{R}^4$ )
$\epsilon$	emissivity
$\theta$	time, $\text{hr}$



$\sigma$  stress, N/cm<sup>2</sup> (lb/in<sup>2</sup>)

$\tau$  strain, cm/cm (in/in)

$\phi$  angle, radians

Subscripts:

c cold

cr critical

h hot

r rim

rc rim cross section

sb support bracket

sink heat sink

ss shadow shield sheet

str shield sheet to rim

v vertical loading

x shield system component

x-x denotes axis

y-y denotes axis

1g denotes a 1-Earth-gravity field

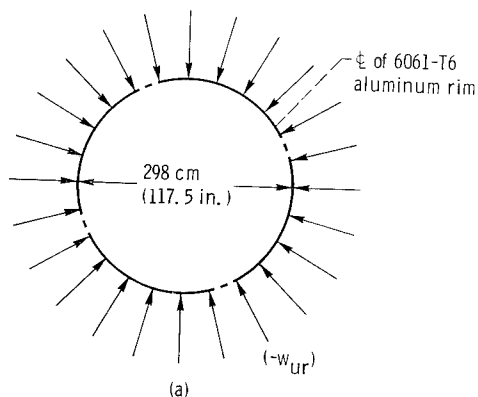
6g denotes six times a 1-Earth-gravity field

## APPENDIX B

### STRUCTURAL ANALYSIS OF SHADOW SHIELD RIM

#### Stability of Rim

The shadow shield rim, shown in sketch a, was made of 6061-T6 aluminum with an outside diameter of 3.8 centimeters (1.5 in.) and a wall thickness of 0.165 centimeter (0.065 in.). The Young's modulus  $E_r$  was  $7.58 \times 10^6$  N/cm<sup>2</sup> ( $1.1 \times 10^7$  psi) and the moment of inertia  $I_r$  was 3.14 cm<sup>4</sup> (0.0754 in<sup>4</sup>).



Consider the rim to be a uniform circular ring under uniform radial loading (ref. 10, p. 343):

$$-w_{ur, cr} = \frac{3E_r I_r}{R_r^3} = 21.5 \text{ N/cm (12.3 lb/in)} \quad (B1)$$

The maximum applied load on the rim during the short-term transient case (table I) due to the contraction between both sheets and the rim is  $-w_{ur} = 26.6$  N/cm (15.2 lb/in). No pretension load was considered. This pretension load was small when the shield sheets were assembled on the aluminum rim. And further, since the shield sheet material is subject to some creep, we expected partial relaxation of any pretension load during the period of time between assembly and testing of the shadow shield.

The result shows that the maximum thermally induced loading on the rim is above the critical loading. However, the shield sheets were joined over the rim by a nonrigid connection device and, further, equation (B1) is a conservative representation of the

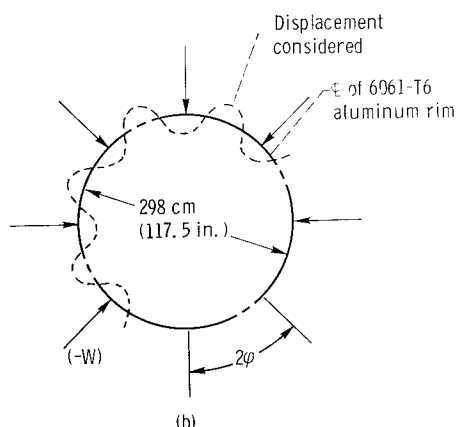
rim loading. Therefore, it was decided (1) that all the 26.6-N/cm (15.2-lb/in) thermal force would not be transferred to the shield rim and (2) that in reality the calculated critical loading of 21.5 N/cm (12.3 lb/in) is low. Both of these decisions led to the supposition that  $w_{ur, cr}$  and  $w_{ur}$  for the imposed extreme transient condition tend to approach one another for this design exercise. The design therefore proceeded, but under the full recognition that the shield rim is structurally marginal for this extreme boundary design condition.

### Radial Displacement of Rim under Load

Consider the uniform rim loading  $w_{ur}$  to be divided into 30 evenly spaced force vectors  $W$ , each acting on the rim at a shield tab location. Since the shield tabs are 3.81 centimeters (1.5 in.) wide, the relation between  $W$  and  $w_{ur}$  is

$$W = \frac{\pi D_r}{30} w_{ur} \quad (B2)$$

Considering outward displacement of the rim only, as shown in sketch b, the result



would be used to determine the extension of the sheet radius (ref. 10, p. 174):

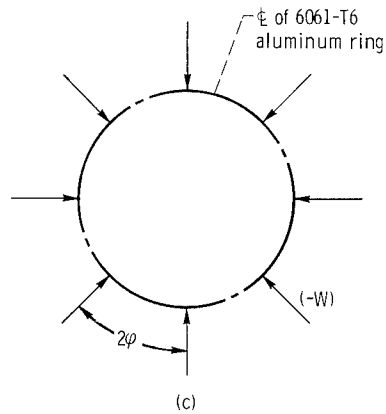
$$\Delta R_r = \frac{WR_r^3}{4E_r I_r} \left( \frac{2}{\phi} - \frac{1}{\sin \phi} - \frac{\phi \cos \phi}{\sin^2 \phi} \right) \quad (B3)$$

The maximum applied load on the rim during the short-term transient case (table I)

due to the contraction between both sheets and the rim is  $-w_{ur} = 26.6 \text{ N/cm}$  (15.2 lb/in). Hence,  $-W = 832 \text{ N}$  (187 lb) and  $\Delta R_r = 0.001085 \text{ cm}$  (0.000427 in.) for outward displacement. This displacement is considered to be negligible.

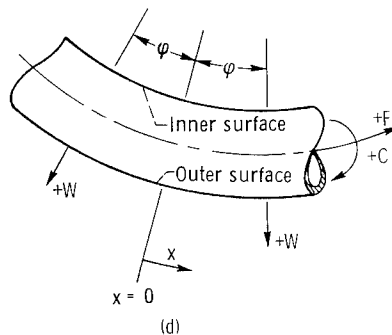
### Stress in Rim Due to Thermal Contraction Force

Again consider the uniform rim loading  $w_{ur}$  to be divided into 30 evenly spaced force vectors  $W$  each acting on the rim at a shield tab location (sketch c), where the



area of the rim cross section  $A_{rc}$  is  $1.884 \text{ cm}^2$  ( $0.292 \text{ in}^2$ ). The expression for the moment  $C$  induced in the rim from  $x = 0$  to  $x = \varphi$  is (ref. 10, p. 174)

$$C = \frac{1}{2} W R_r \left( \frac{\cos x}{\sin \varphi} - \frac{1}{\varphi} \right) \quad (B4)$$



The circumferential force induced in the rim (sketch d) at each load point is (ref. 10, p. 174):

$$F = \frac{1}{2} W(\cot \varphi) \quad (B5)$$

and at the point exactly between loads is (ref. 10, p. 174):

$$F = \frac{1}{2} W \left( \frac{1}{\sin \varphi} \right) \quad (B6)$$

The developed equations representing the stress  $\sigma$  on the inner and outer surfaces at the load points as well as between the load points are

(1) For the inner surface of the rim at load points:

$$\sigma = \frac{W}{2A_{rc}} (\cot \varphi) + \frac{WR_r}{2} \left( \frac{\cos x}{\sin \varphi} - \frac{1}{\varphi} \right) \frac{d_{rc}}{2I_r} \quad (B7)$$

(2) For the outer surface at load points:

$$\sigma = \frac{W}{2A_{rc}} (\cot \varphi) - \frac{WR_r}{2} \left( \frac{\cos x}{\sin \varphi} - \frac{1}{\varphi} \right) \frac{d_{rc}}{2I_r} \quad (B8)$$

(3) For the inner surface between load points:

$$\sigma = \frac{W}{2A_{rc}} \left( \frac{1}{\sin \varphi} \right) + \frac{WR_r}{2} \left( \frac{\cos x}{\sin \varphi} - \frac{1}{\varphi} \right) \frac{d_{rc}}{2I_r} \quad (B9)$$

(4) For the outer surface between load points:

$$\sigma = \frac{W}{2A_{rc}} \left( \frac{1}{\sin \varphi} \right) - \frac{WR_r}{2} \left( \frac{\cos x}{\sin \varphi} - \frac{1}{\varphi} \right) \frac{d_{rc}}{2I_r} \quad (B10)$$

When the numerical values of the variables are inserted for each case, these equations become

(1) For the inner surface of the rim at load points:

$$\left. \begin{aligned} \sigma &= W(-0.742) && \text{(SI units)} \\ \sigma &= W(-4.791) && \text{(U. S. customary units)} \end{aligned} \right\} \quad (B11)$$

(2) For the outer surface at load points:

$$\left. \begin{aligned} \sigma &= W(5.792) && \text{(SI units)} \\ \sigma &= W(37.374) && \text{(U. S. customary units)} \end{aligned} \right\} \quad (B12)$$

(3) For the inner surface between load points:

$$\left. \begin{aligned} \sigma &= W(4.174) && \text{(SI units)} \\ \sigma &= W(26.932) && \text{(U. S. customary units)} \end{aligned} \right\} \quad (B13)$$

(4) For the outer surface between load points:

$$\left. \begin{aligned} \sigma &= W(0.904) && \text{(SI units)} \\ \sigma &= W(5.831) && \text{(U. S. customary units)} \end{aligned} \right\} \quad (B14)$$

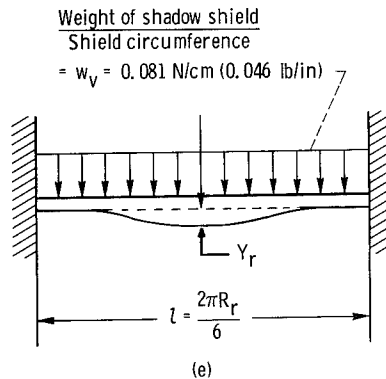
The applied load on the rim during the short-term cooldown transient phase (table I) due to the contraction between both sheets and the rim is  $-w_{ur} = 26.6 \text{ N/cm}$  (15.2 lb/in). Hence,  $-W = 832 \text{ N}$  (187 lb). The results of equations (B11) to (B14) may be tabulated as follows:

	At load points	Between load points
Resultant stress on rim inner surface, $\text{N/cm}^2$ (psi)	+618 (+896), tension	-3472 (-5036), compression
Resultant stress on rim outer surface, $\text{N/cm}^2$ (psi)	-4819 (-6989), compression	-752 (-1090), compression

The stresses are well below the yield point ( $27.6 \times 10^3 \text{ N/cm}^2$ ;  $40 \times 10^3 \text{ psi}$ ) of 6061-T6 aluminum alloy. Hence, the rim design was considered to be adequate.

### Vertical Deflection of Rim

Consider one segment of the rim as a uniformly loaded beam with both ends fixed (sketch e). The maximum deflection is (ref. 10, p. 112):



$$Y_r = \frac{1}{384} \frac{w_v l^4}{E_r I_r} \quad (\text{B15})$$

Under 1-g loading,  $Y_r$  is 0.0053 centimeter (0.0021 in.). Under 6-g loading,  $Y_r$  is 0.0320 centimeter (0.0126 in.).

The stress due to bending at the center of the span is (ref. 10, p. 112):

$$\sigma = \frac{1}{12} w_v l^2 \left( \frac{d}{21} \right) \quad (\text{B16})$$

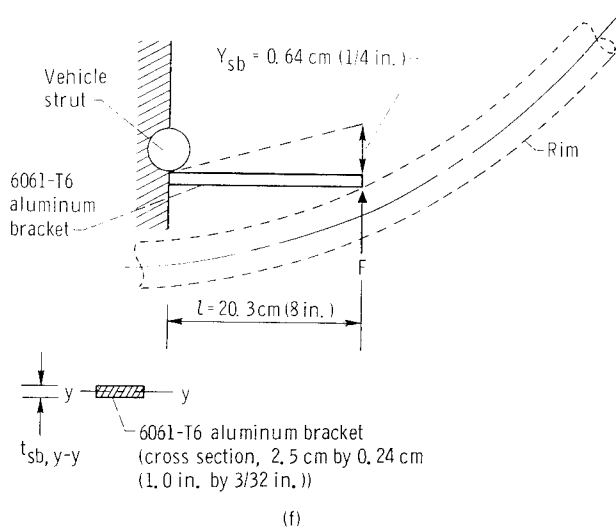
Under a 1-g loading,  $\sigma$  is  $103 \text{ N/cm}^2$  (149 psi). Under a 6-g loading,  $\sigma$  is  $616.5 \text{ N/cm}^2$  (894 psi). Again, these values are less than the yield stress for the 6061-T6 rim material.

## APPENDIX C

### STRESS AND DISPLACEMENT OF SUPPORT BRACKET

#### In-Plane Condition

During the null test, the rim shrinks about 0.64 centimeter (1/4 in.) in the radial direction (sketch f).



The load  $F$  that is imposed on the end of the bracket may be calculated as follows (ref. 10, p. 104):

$$F = \frac{3Y_{sb} E_r I_{sb, y-y}}{l^3} \quad (C1)$$

The maximum stress at the strut may be expressed as

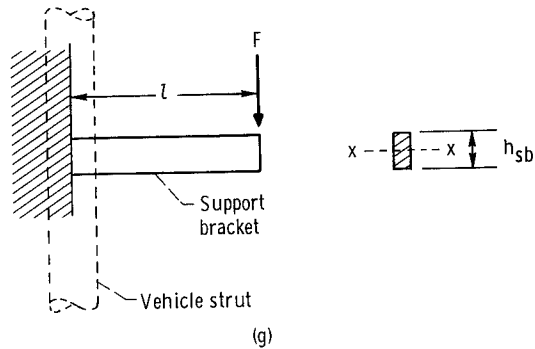
$$\sigma = \frac{F l t_{sb}}{2 I_{sb, y-y}} = 4164 \text{ N/cm}^2 \text{ (6040 psi)}$$

where  $t_{sb, y-y}$  is 0.24 centimeter (3/32 in.) and  $I_{sb, y-y}$  is  $2.855 \times 10^{-3} \text{ cm}^4$  ( $6.86 \times 10^{-5} \text{ in}^4$ ).



## Vertical Loading under a 6-g Load

The vertical loading (sketch g) is determined from



the shield mass divided by the number of struts (in this case, twelve). At 1-g, the loading is 6.30 newtons per strut (1.416 lb/strut). At 6 g's, the loading is 37.8 newtons per strut (8.495 lb/strut). The stress at a strut may be expressed as

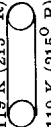
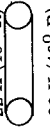
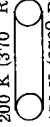
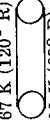
$$\sigma = \frac{Flh_{sb}}{2I_{sb, x-x}} = 3004 \text{ N/cm}^2 (4357 \text{ psi})$$

where  $h_{sb}$  is 2.5 centimeters (1 in.) and  $I_{sb, x-x}$  is  $0.325 \text{ cm}^4$  ( $0.78 \times 10^{-2} \text{ in}^4$ ). This is still well below the yield point of 6061-T6 aluminum.

## REFERENCES

1. Propellant Selection for Spacecraft Propulsion Systems. Volume 2: Missions and Vehicles. (K-19-68-6, V. 2, Lockheed Missiles and Space Co.; NASw-1644) NASA CR-96988, 1968.
2. Oglebay, John C.; Sagerman, Gary D.; and Valentine, Harold H.: Analytic Evaluation of Space Storable Propellants for Unmanned Jupiter and Saturn Orbiter Missions. NASA TM X-1793, 1969.
3. Knoll, R. H.; and Oglebay, John C.: Lightweight Thermal Protection Systems for Space Vehicle Propellant Tanks. SAE Paper 746C, Sept. 1963.
4. Boyle, Robert J.; and Knoll, Richard H.: Thermal Analysis of Shadow Shields and Structural Members in a Vacuum. NASA TN D-4876, 1968.
5. Knoll, Richard H.; and Bartoo, Edward R.: Experimental Studies on Shadow Shields for Thermal Protection of Cryogenic Tanks in Space. NASA TN D-4887, 1968.
6. Boyle, Robert J.; and Stochl, Robert J.: Analytic and Experimental Evaluation of Shadow Shields and Their Support Members for Thermal Control of Space Vehicles. NASA TN D-7612, 1974.
7. DeWitt, Richard L.; and Boyle, Robert J.: Thermal Performance of an Integrated Thermal Protection System for Long-Term Storage of Cryogenic Propellants in Space. NASA TN D-8320, 1976.
8. Williams, L. R.; Young, J. D.; and Schmidt, E. H.: Design and Development Engineering Handbook of Thermal Expansion Properties of Aerospace Materials at Cryogenic and Elevated Temperatures. (R-6981, Rocketdyne; NAS8-19) NASA CR-102331, 1969.
9. Synge, John L.; and Griffith, Byron A.: Principles of Mechanics. 2nd ed., McGraw-Hill Book Co., Inc., 1949.
10. Roark, Raymond J.: Formulas for Stress and Strain. 4th ed., McGraw-Hill Book Co., Inc., 1965.

TABLE 1. - THERMALLY INDUCED FORCES ON SHADOW SHIELD SHEETS

Test phase	Design condition	Shield	Component	Material	Direction (if applicable)	Component temperature		Contraction relative to 289 K (520° R) from fig. 9, cm/cm (or in/in)	Contraction relative to rim, $\epsilon_{6061-T6} - \epsilon_{X-850}$ , cm/cm (or in/in)	Average contraction, cm/cm (or in/in)	Definition of sheet condition relative to rim	Uniformly spaced load produced in rim by a single sheet, from fig. 5, $w_{ur}/2$	
						K	°R					N/cm	lb/in
1	Cooldown transient 119 K (215° R) 216 K  (388° R) 119 K (215° R)	Both	Sheets	X-850	Roll	119	215	-43.2×10 <sup>-4</sup>	26.1×10 <sup>-4</sup>	34.4×10 <sup>-4</sup>	Short-term tight	a13.3	a7.6
			Rim	6061-T6	Cross-roll	119	215	-59.8	42.7				
2	Null steady state 22 K (40° R) 22 K  (40° R) 22 K (40° R)	Both	Sheets	X-850	Roll	22	40	-58.0×10 <sup>-4</sup>	13.6×10 <sup>-4</sup>	25.6×10 <sup>-4</sup>	-----	a9.8	a5.6
			Rim	6061-T6	Cross-roll	22	40	-82.0	37.6				
3	Space steady state 200 K (370° R) 111 K  (200° R) 150 K (270° R)	Payload	Sheets	X-850	Roll	206	370	-22.7×10 <sup>-4</sup>	-13.8×10 <sup>-4</sup>	-1.25×10 <sup>-4</sup>	Loose	a, b0	a, b0
			Rim	6061-T6	Cross-roll	150	270	-36.8	.3				
3	Space steady state 67 K (120° R) 33 K  (60° R) 33 K (60° R)	Tank	Sheets	X-850	Roll	67	120	-52.3×10 <sup>-4</sup>	8.4×10 <sup>-4</sup>	21.6×10 <sup>-4</sup>	Long-term tight	a8.4	a4.8
			Rim	6061-T6	Cross-roll	33	60	-56.7	12.8				
						67	120	-73.2	29.3				
						33	60	-79.8	35.9				
						33	60	-43.9	0				

<sup>a</sup>Liquid-nitrogen curve in fig. 5 was used.<sup>b</sup>Pretension required.

TABLE II. - WEIGHT BREAKDOWN OF A DOUBLE-SHEETED  
SHADOW SHIELD ASSEMBLY

Item	Quantity	Weight	
		kg	lb
Schjeldahl X-850 sheet	2	1.10	2.44
Aluminum rim	1	4.80	10.58
Aluminum support brackets	6	.79	1.75
Stainless-steel bolts (to attach brackets to rim)	12	.46	1.01
Stainless-steel bolts (to attach brackets to vehicle structure)	24	.23	.50
Aluminum hollow pins (load spreaders in sheet tabs)	72	.20	.45
Brass bolt assemblies (for attaching sheet tabs and sheet tensioning)	36	.67	1.48
	Total	8.25	18.21

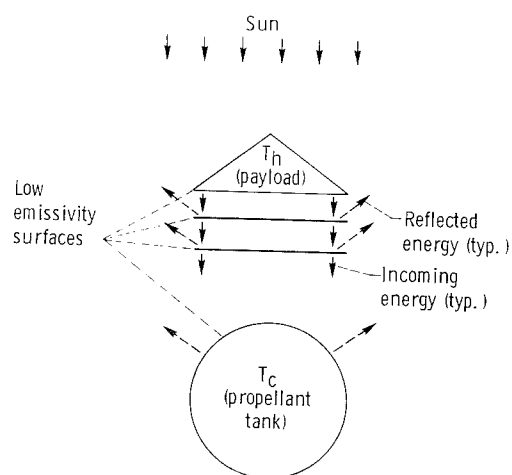


Figure 1. - Schematic of shadow shield system operation.  
Space vacuum and temperature (0 K; 0° R) environment assumed.

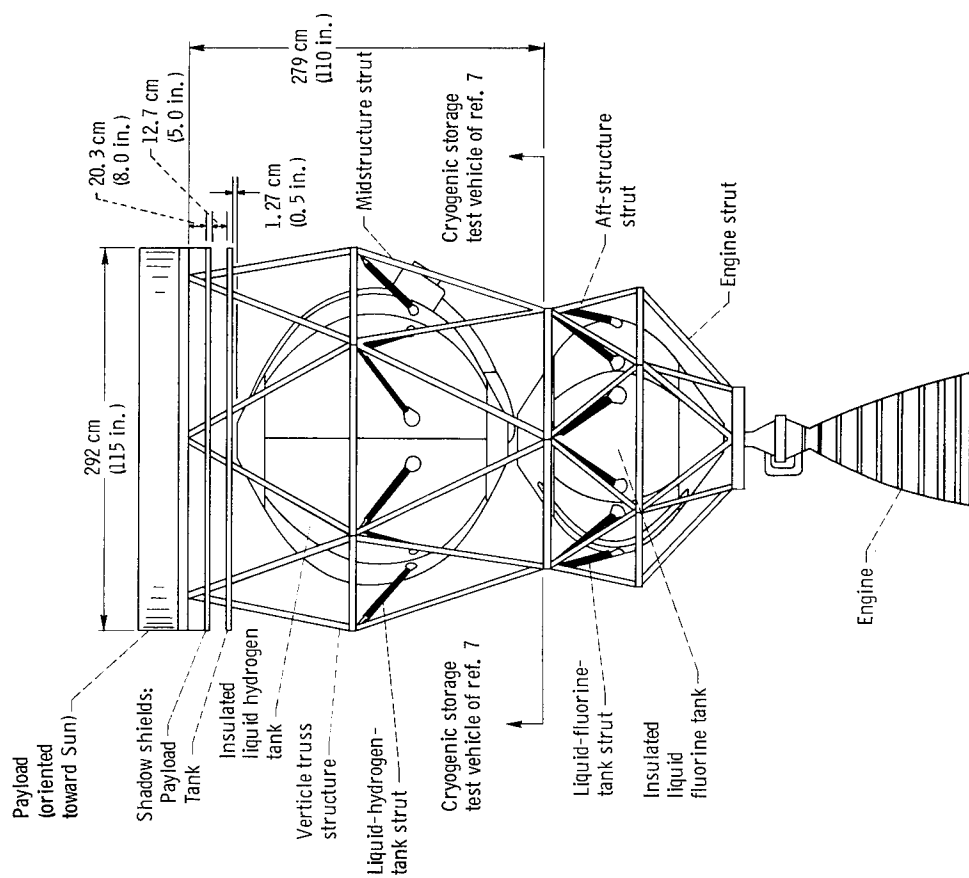


Figure 2. - Conceptual design of hydrogen-fluorine stage.

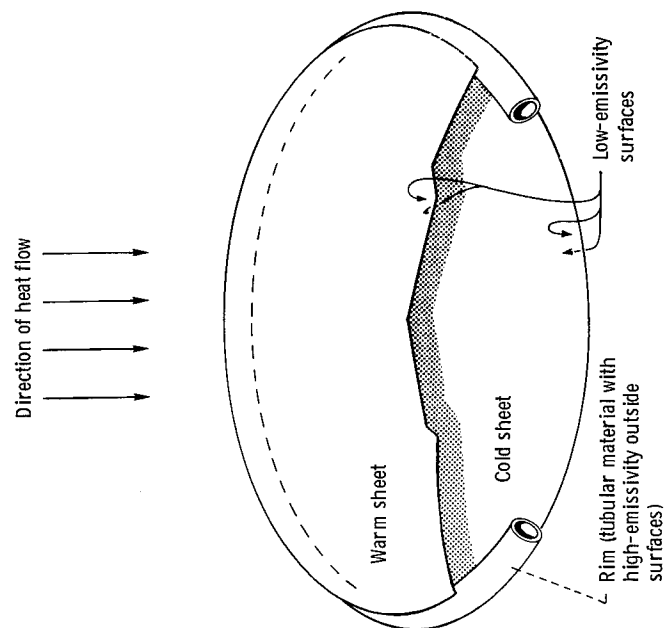


Figure 3. - Sketch of double-sheeted shadow shield.

	Initial temperatures	Test phase		
		Cooldown transient	Null steady state	Space steady state
Payload	289 K (520° R)	289 K → 22 K (520° R → 40° R)	22 K (40° R)	289 K (520° R)
Shield adjacent to payload	289 K (520° R) 289 K (520° R) 289 K (520° R)	119 K (215° R) 119 K (215° R) 216 K (388° R)	22 K (40° R) 22 K (40° R) 22 K (40° R)	206 K (370° R) 150 K (270° R) 111 K (200° R)
Shield adjacent to tank	289 K (520° R) 289 K (520° R) 289 K (520° R)	119 K (215° R) 119 K (215° R) 216 K (388° R)	22 K (40° R) 22 K (40° R) 22 K (40° R)	67 K (120° R) 33 K (60° R) 33 K (60° R)
Surrounding environmental temperature	289 K (520° R)	289 K → 22 K (520° R → 40° R)	22 K (40° R)	22 K (40° R)

Figure 4. - Shadow shield design temperature conditions for CSTV test program.

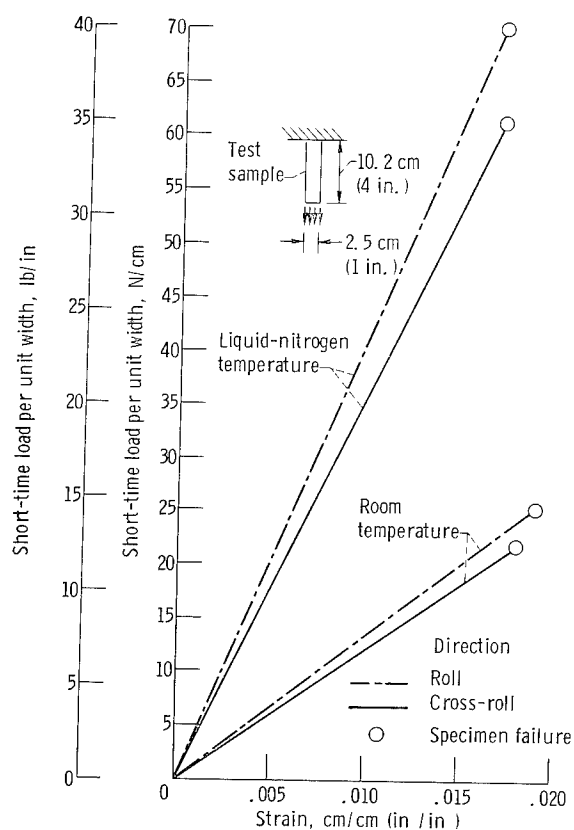


Figure 5. - Tensile load and strain relations for Schjeldahl X-850.

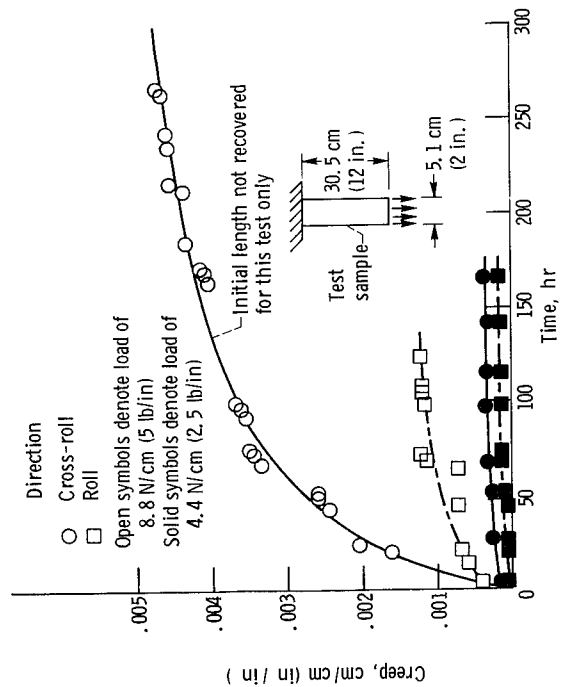


Figure 6. - Elongation of Schjeldahl X-850 as function of time under constant tensile loading. (Testing conducted in ambient temperature and pressure.)

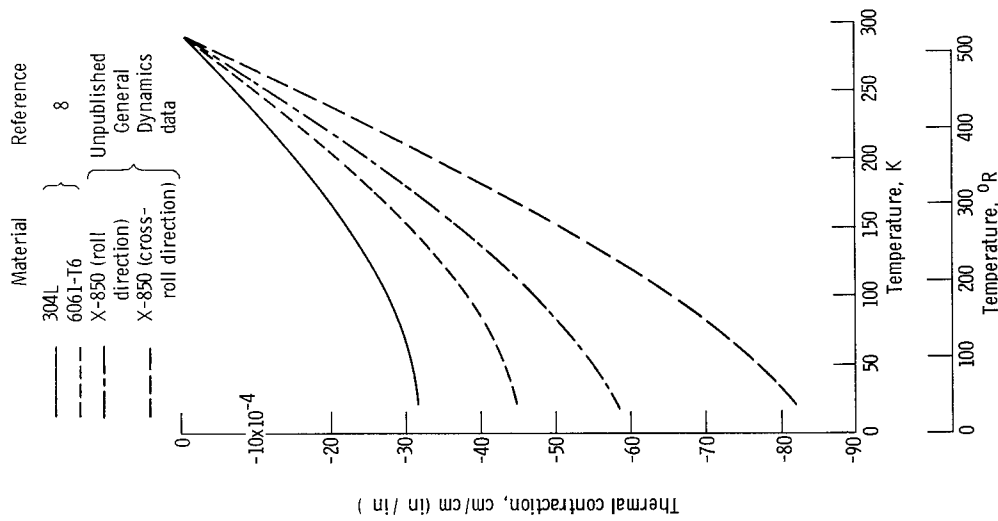


Figure 7. - Thermal contractions of 304L stainless steel, 6061-T6 aluminum, and Schjeldahl X-850 as functions of temperature.

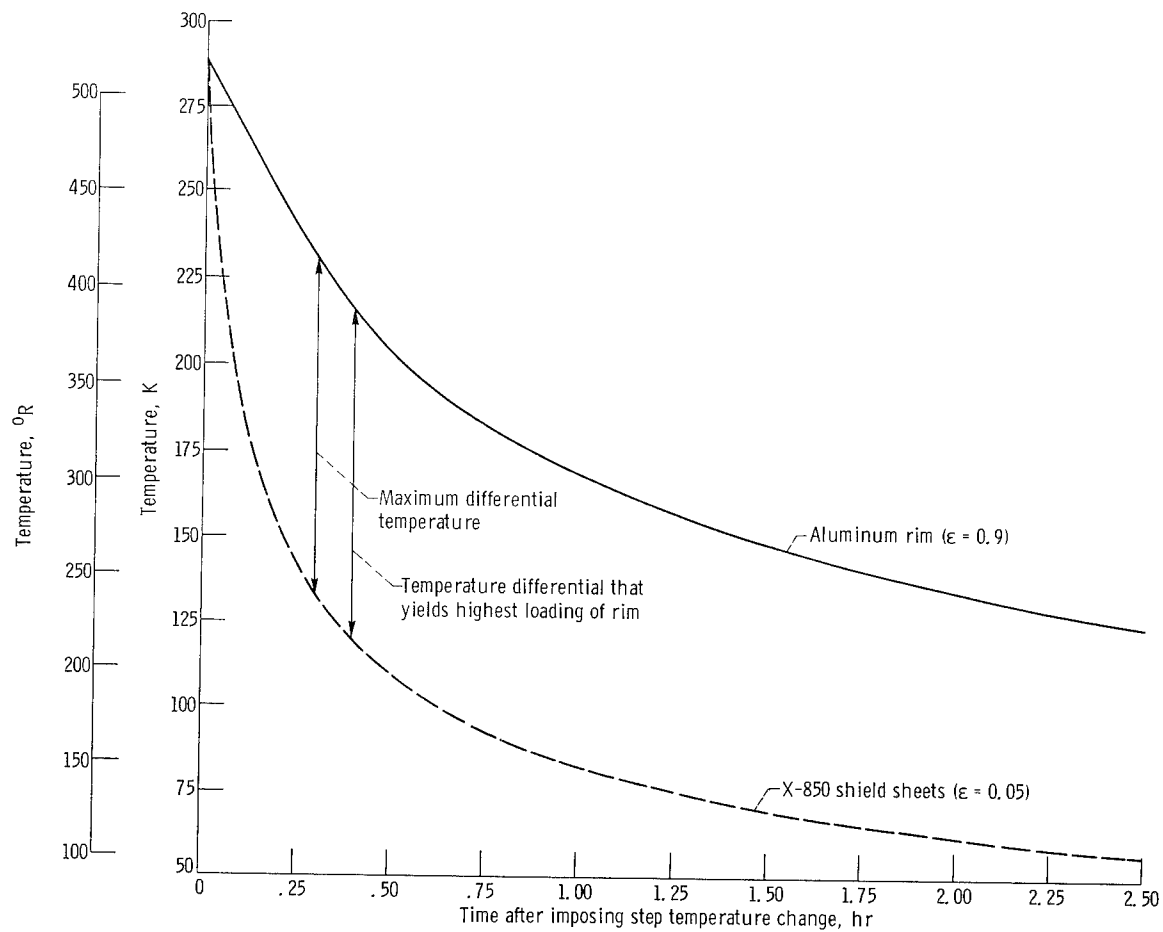


Figure 8. - Radiation chilldown of shadow shield rim and sheets when exposed to a step change from 289 K (520° R) to 22 K (40° R) in surrounding temperature.



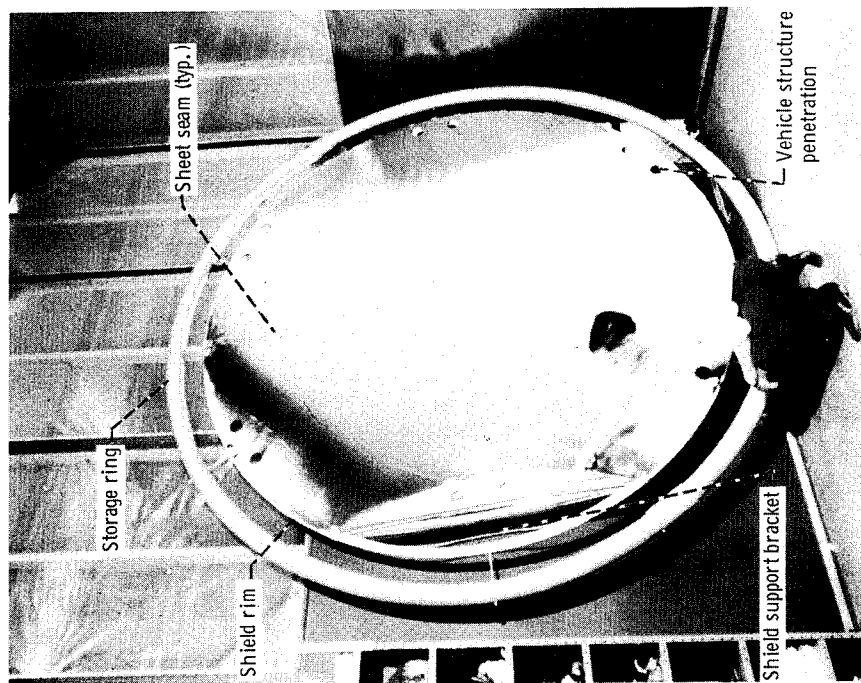


Figure 10. - Shadow shield for use in CSTV program.

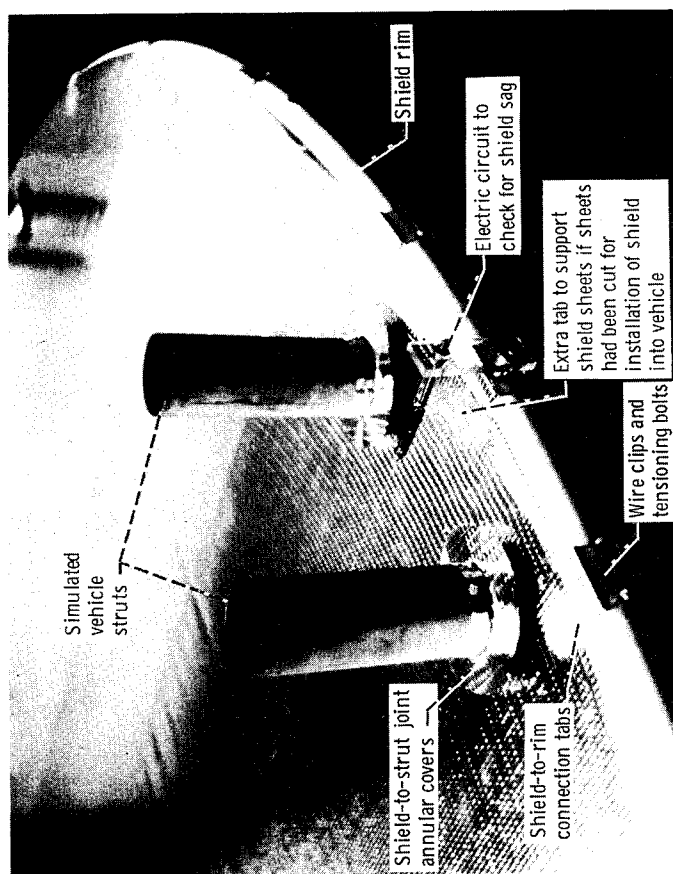


Figure 9. - Prototype shadow shield mounted on simulated vehicle struts.

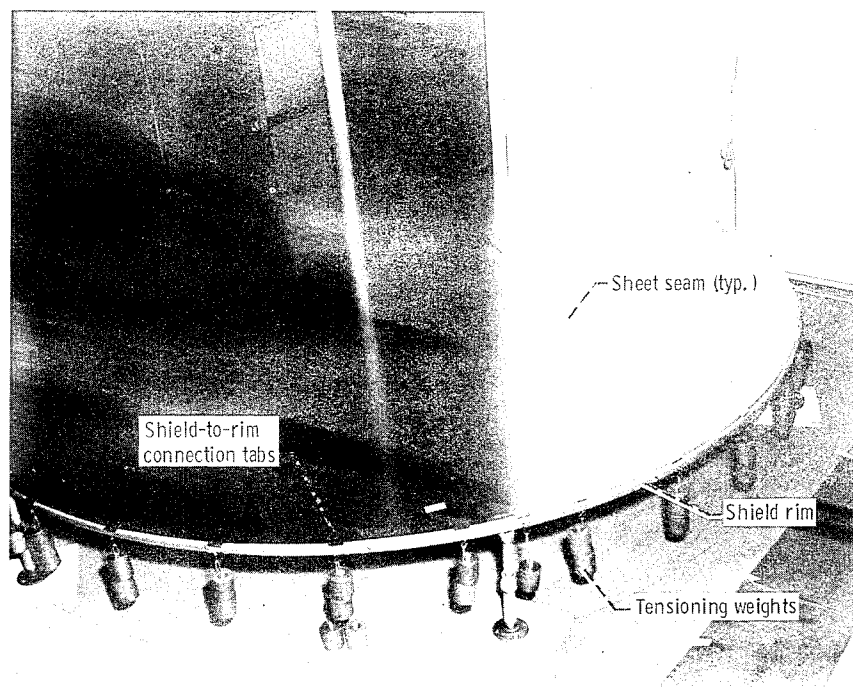


Figure 11. - Shadow shield sheet being stretched prior to assembly on rim.

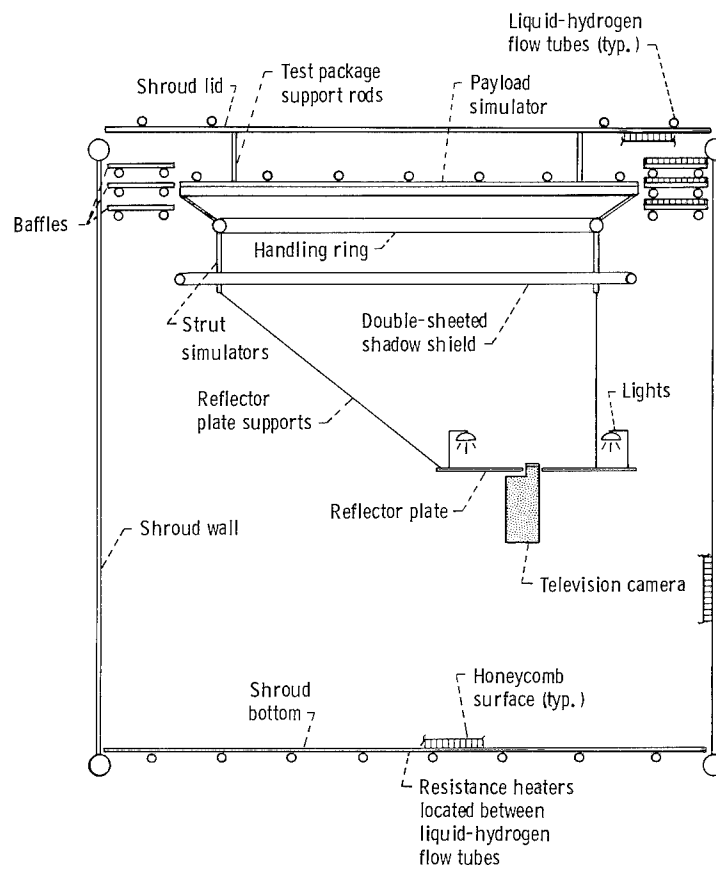


Figure 12. - Schematic drawing of major pieces of test hardware.

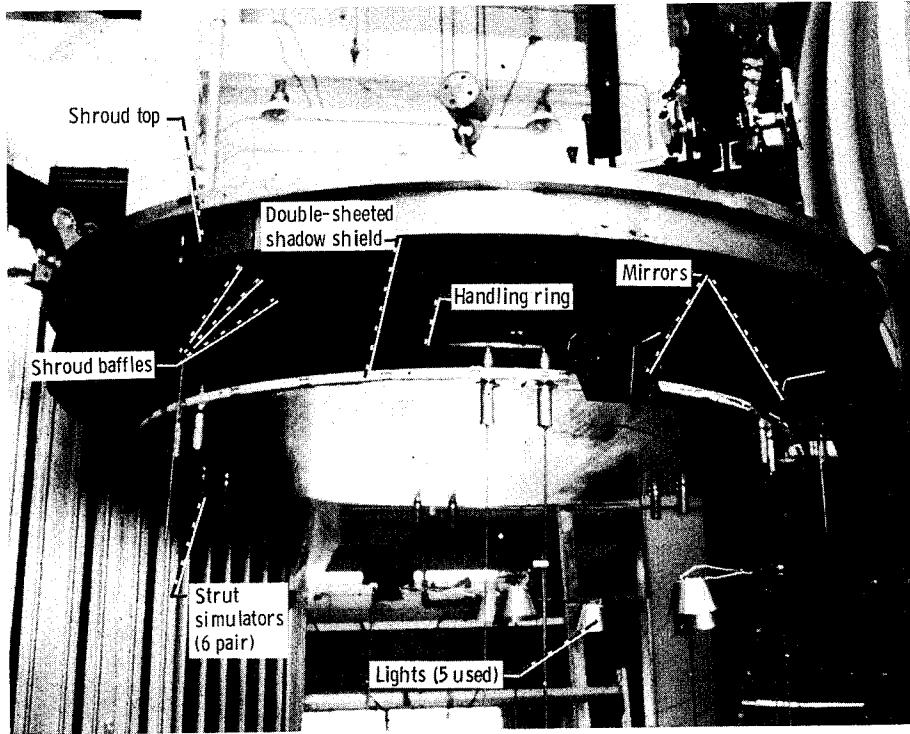


Figure 13. - Double-sheeted shadow shield mounted from shroud lid. (Reflector plate and television camera are below frame of picture.)

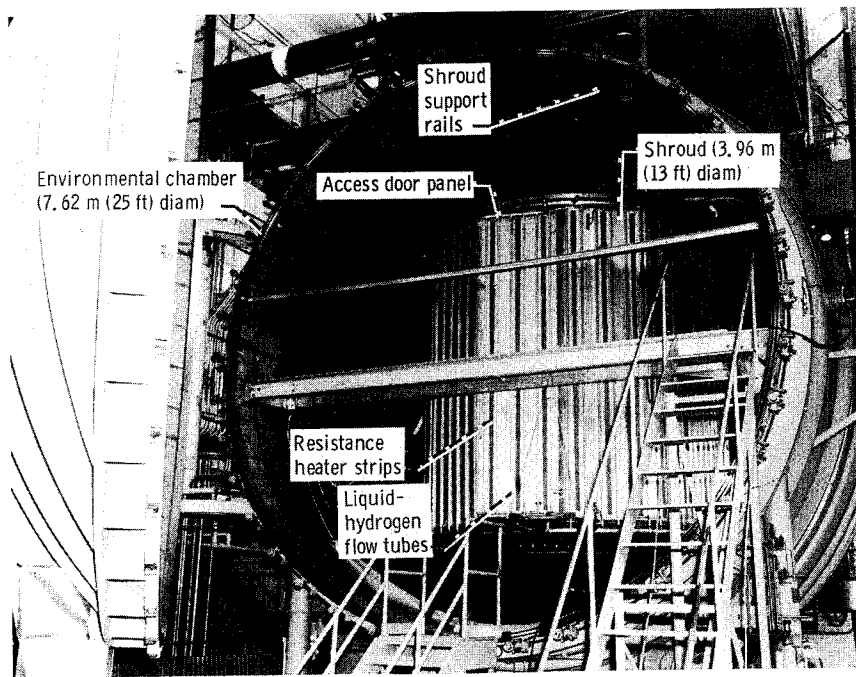
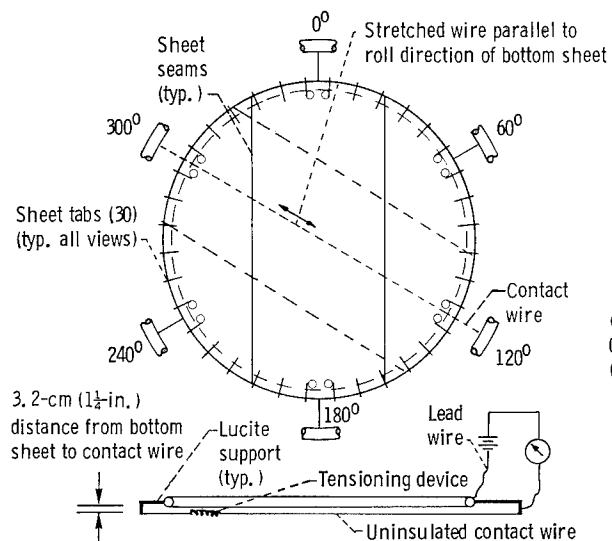
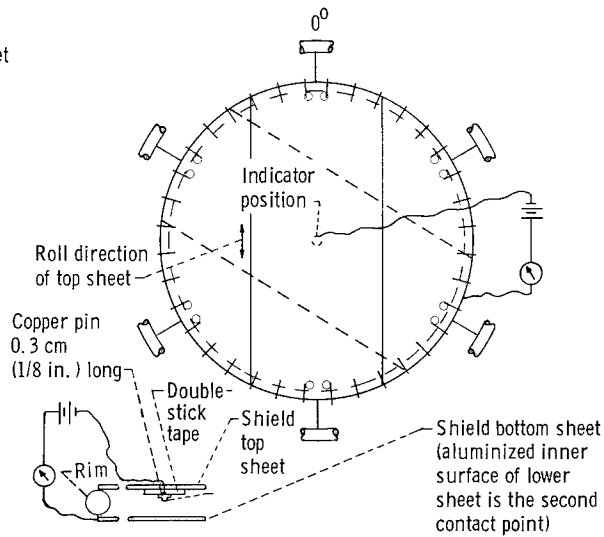


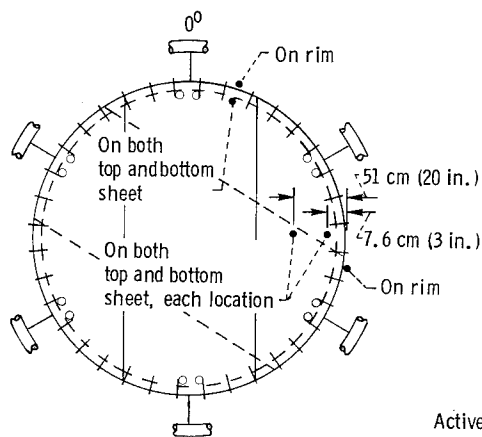
Figure 14. - Shroud inside environmental chamber.



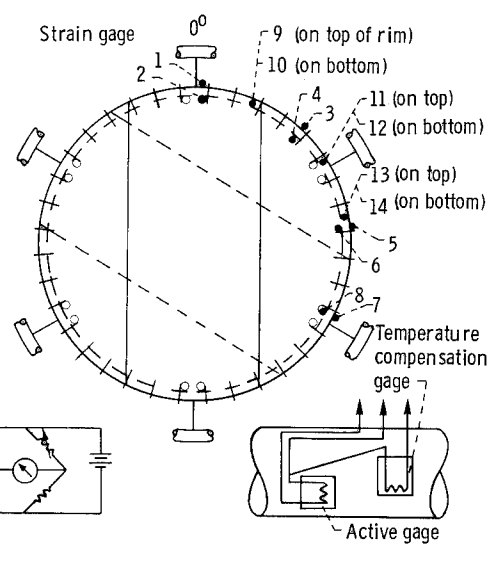
(a) Short-circuit wire.



(b) Sheet contact circuit.

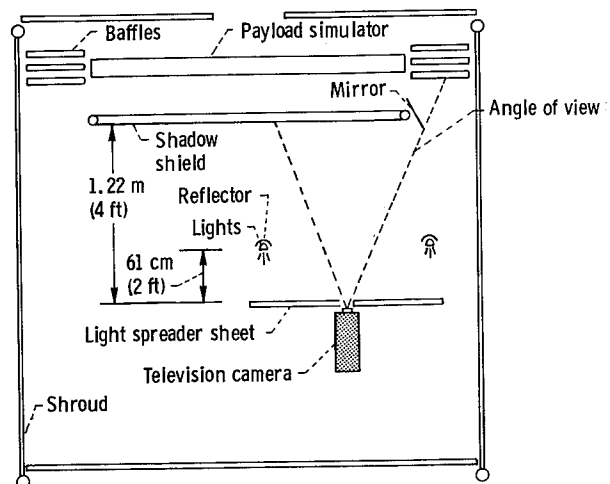
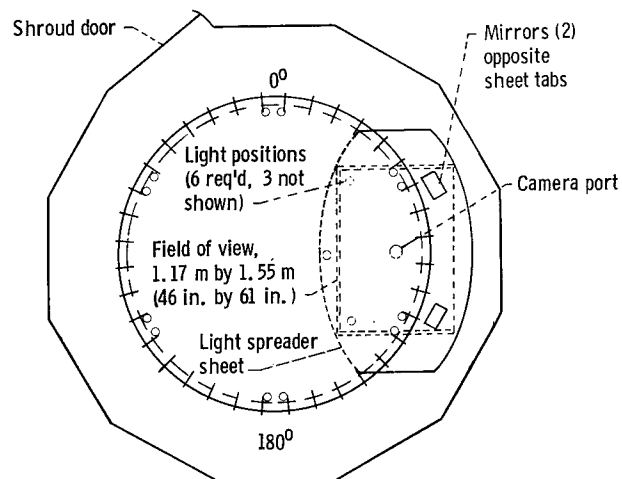


(c) Thermocouple locations.



(d) Strain gages.

Figure 15. - Instrumentation arrangement on assembled shadow shield.



(e) Television package.

Figure 15. - Concluded.

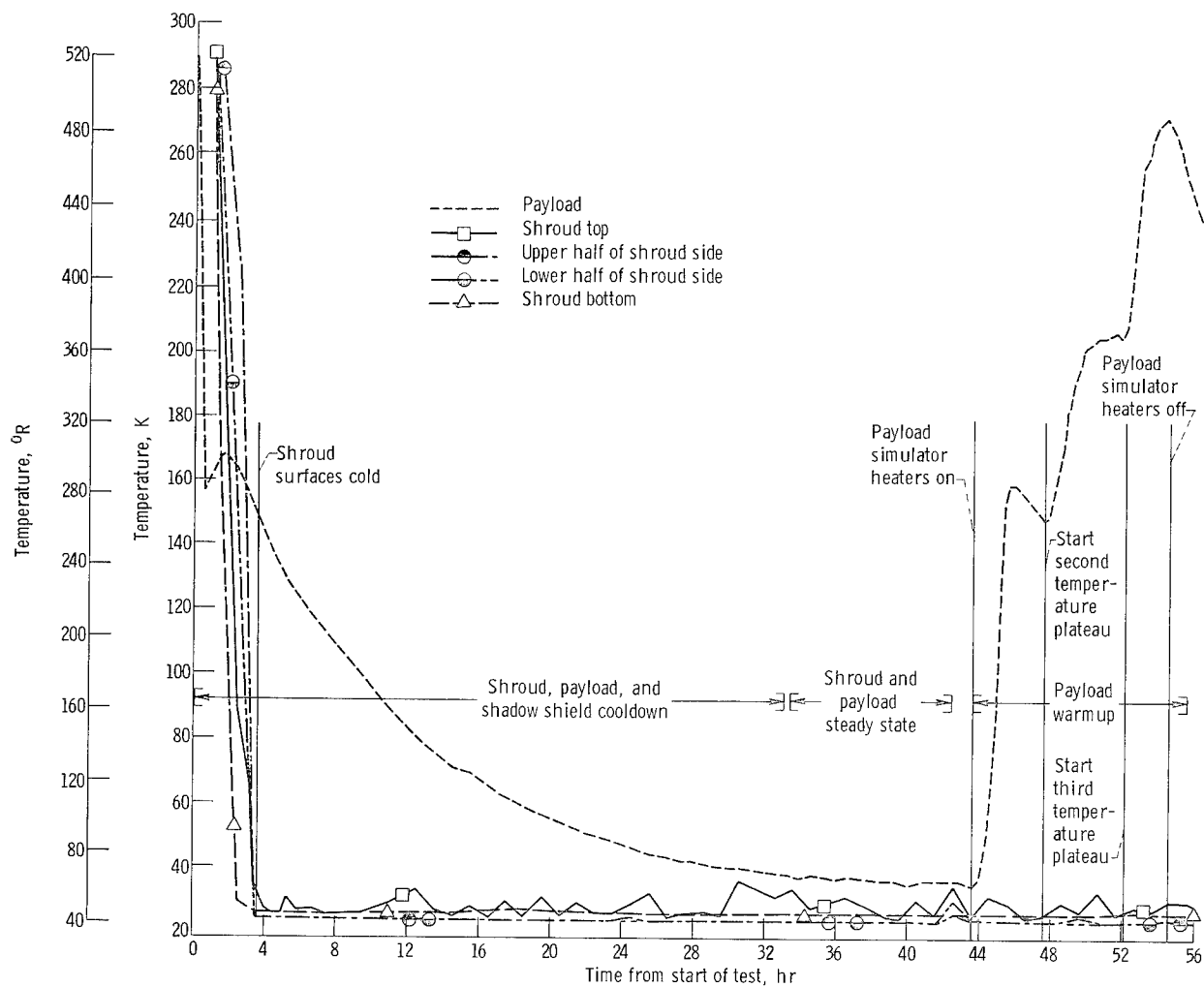


Figure 16. - Average shroud and payload simulator temperatures as functions of time during the testing period.

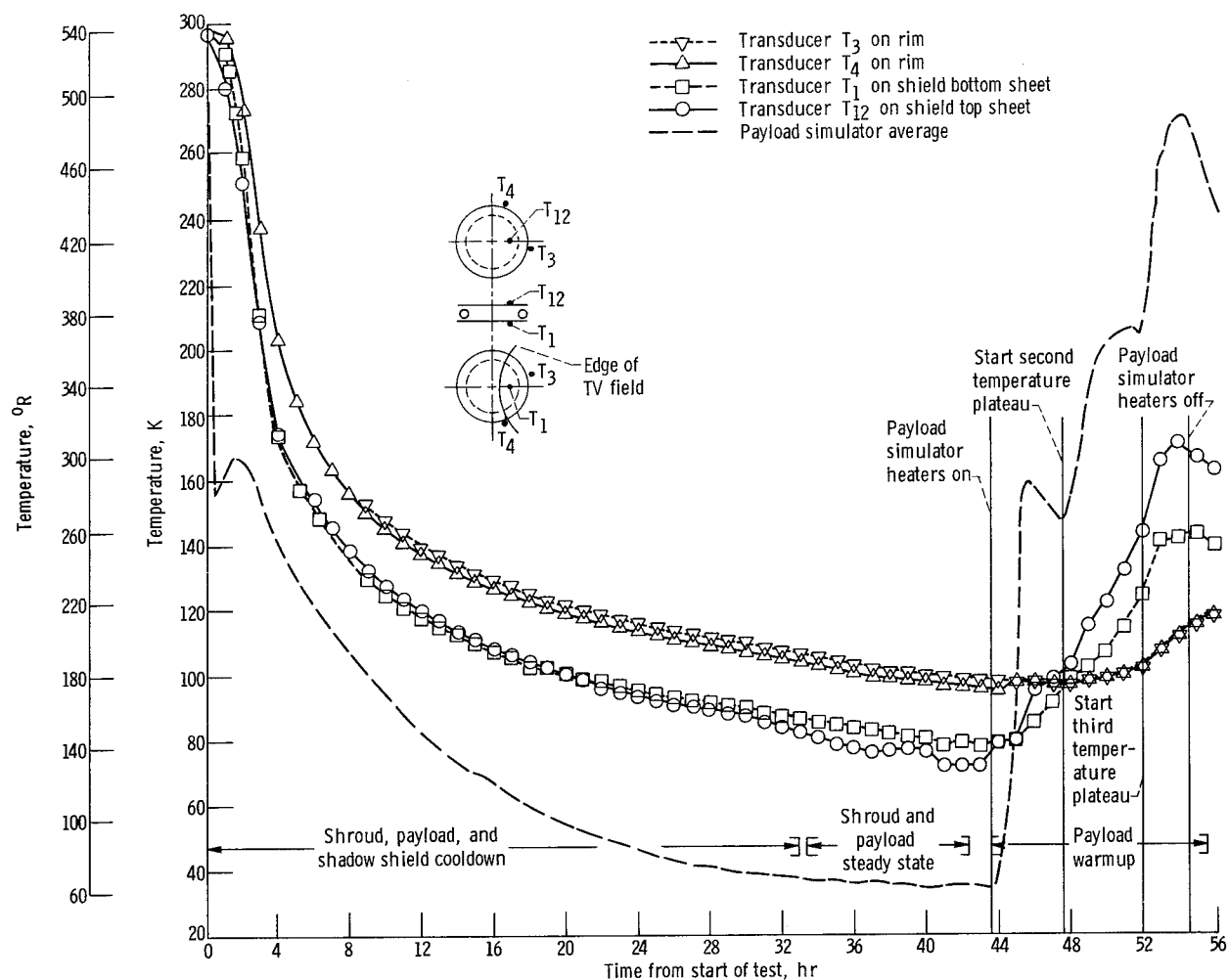


Figure 17. - Shield sheet and rim temperatures as functions of time during the testing period. (Temperature differential from sheets to rim,  $\Delta T_{str} = T_3 - (T_{12} + T_1)/2$ .)

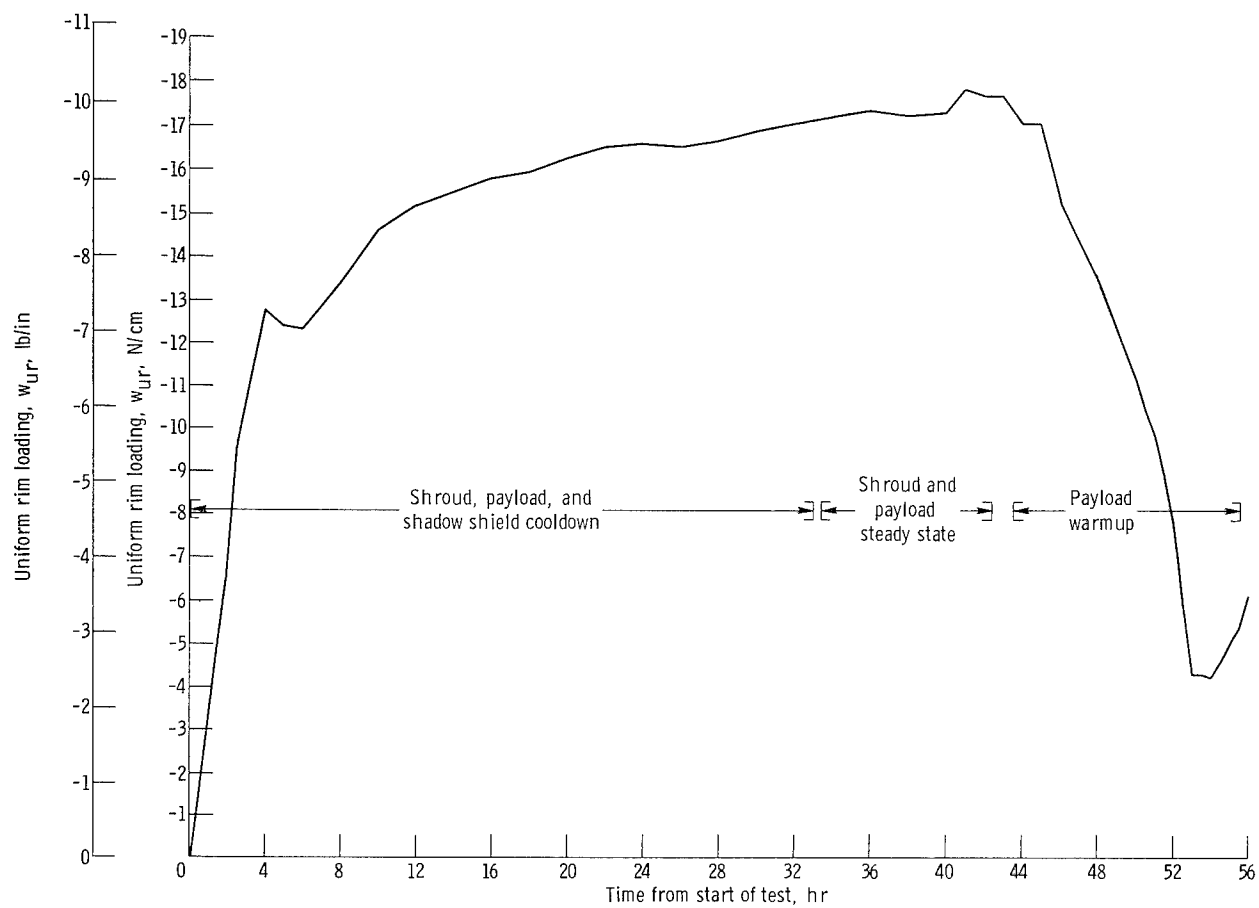


Figure 18. - Calculated uniform rim loading per unit width of rim as function of time during the testing period. (Negative sign implies that the radial load  $w_{UR}$  is directed toward the center of the shadow shield assembly.)



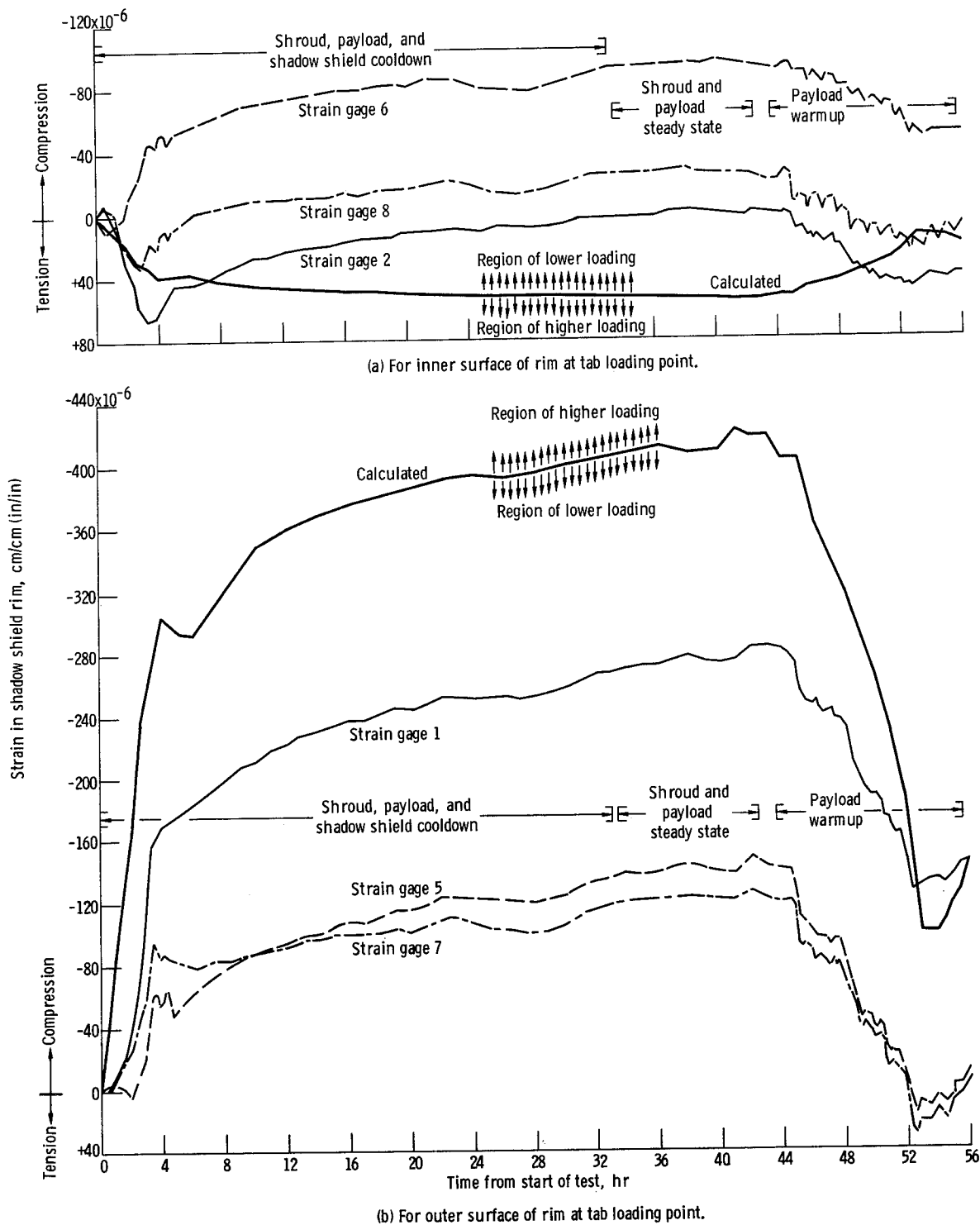


Figure 19. - Calculated and experimentally measured strain histories in the shadow shield rim during the testing period.

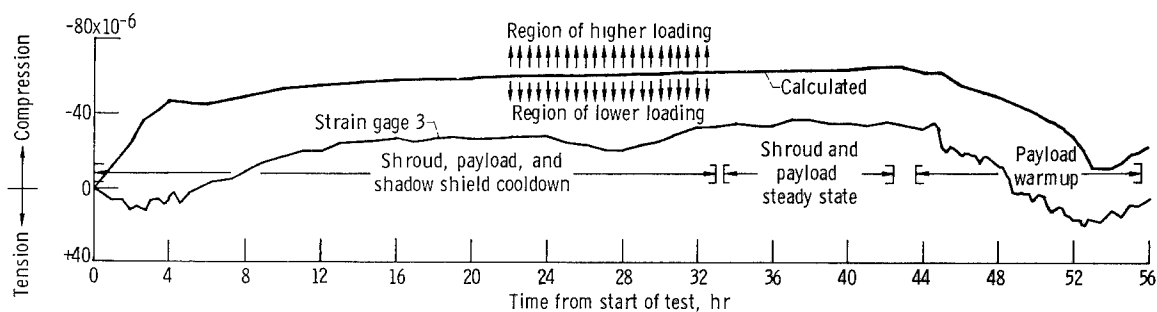
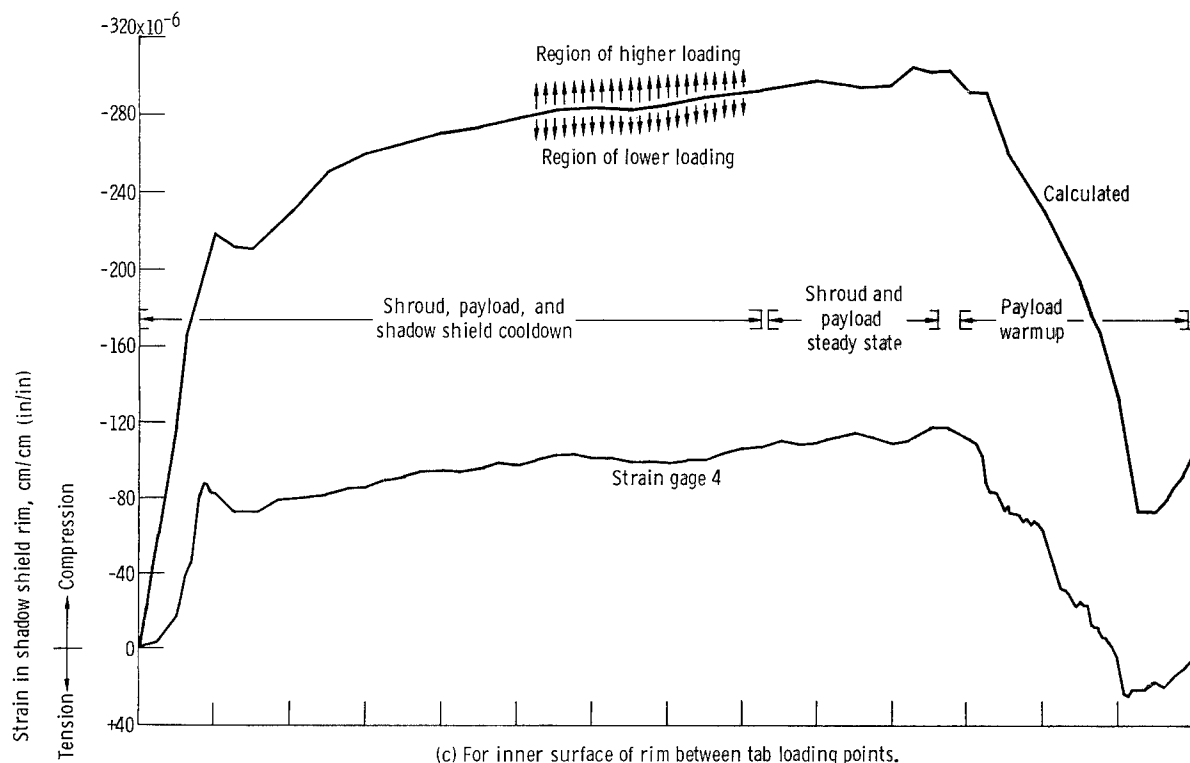


Figure 19. - Concluded.